Small-Scale Cryogenic Refrigeration Technology: Small Scale Pulse Tube Refrigerator

SBIR Phase I Contract W9113M-07-C-0203

Draft Final Report
February 12, 2008

Thomas M. Crittenden
tom.crittenden@vastechnologies.com
Virtual AeroSurface Technologies. Inc.
575 14th Street, Ste. 1375
Atlanta, GA 30318
404-881-8276

S. Mostafa Ghiaasiaan
mghiaasiaan@gatech.edu
Georgia Institute of Technology
Woodruff School of Mechanical Engineering
771 Ferst Drive, Rm. 309
Atlanta, GA 30332-0405
404-894-3746

TABLE OF CONTENTS

LIST OF FIGURES

SUMMARY

The present Phase I STTR program was focused on an investigation into the development and adaptation of pulse tube refrigerator (PTR) cryocoolers to the meso- and micro-scales. Critical challenges for this development include the increasing effects of adverse scale sensitive phenomenon (such as frictional, parasitic heat losses, and adverse heat conduction caused by large temperature gradients) at reduced sizes and their remediation; proper material including fine-structure filler matrices for heat exchangers and regenerators; fabrication techniques; and changes to critical operating parameters such as oscillation frequency which are significantly different than operating parameters of large PTR systems. Some of these phenomena and parameters are inadequately considered in existing design methods and numerical modeling codes (such as Sage) intended for use with full-scale PTRs, furthermore. In the current research, CFD based models were developed using FLUENT to try to remedy some of these deficiencies and allow for more accurate modeling at smaller scales. The Sage code was used for scoping analysis and in order to provide a baseline starting point for the design of the PTR systems. Full CFD modeling was then performed for the refinement of the designs and predicted performance, and for the validation of the initial designs. CFD simulations are also planned for further optimization of the designed systems in the follow – up Phase II investigation. As part of the effort for developing accurate models, closure relations were also developed based upon experimental characterization of the fine mesh filler materials that were found to be appropriate for use in meso and micro scale heat exchangers and regenerators. The characterization of these materials (325 mesh phosphor bronze and 635 mesh stainless steel) was done for properties representing axial and radial flow directions for steady and oscillating flows. The final full CFD simulation and optimization will ultimately be based upon these values. Simultaneously, a manufacturing feasibility study has been carried out for the prototyping of a meso-scale PTR. The material selection for this prototype was completed (using primarily PEEK and silver) and prototype components were fabricated to demonstrate the suitability of the selected materials and fabrication/assembly techniques. These components have been assembled and verified under the pressure range expected for the device operation. In

addition, a vacuum dewar test cell was fabricated for actual experimental tests of the device. Extensive and detailed tests will commence under a Phase II follow-on program. Fabrication, testing and demonstration of functioning meso and micro scale PTRs will be undertaken under a Phase II follow – on program. We expect to construct and test a number of meso scale PTR systems, aimed at examining the effects of variations to the overall design. This will be in addition to tests in which component-level variations will be examined.

1. INTRODUCTION

Stirling Cycles and Pulse Tube Cryocoolers (PTRs) (presented schematically in Fig. 1.1) are widely applied for cryocooling. PTRs are rugged and reliable cryogenic coolers with no moving parts on their cooled ends. Improvement of the efficiency and other performance parameters of PTRs remains a subject of interest, and a number of new and innovative design variations to the basic PTR have been proposed in the recent past. Intensive research has also been underway for decades, aimed at understanding the basic PTR phenomena, improving their performance and efficiency, and developing models for predicting their performance. Analytical tools with various degrees of sophistication are now available for PTRs. However, even the most advanced design tools [e.g., Gideon, 1999 and Yu, Wang, and Zhou, 1998] are typically one-dimensional, and rely on constitutive and closure relations that are at best crude approximations for the complex and periodic flow conditions in PTRs. In this respect, the thermal-hydraulic phenomena in the regenerator component of PTRs are particularly important. Improved understanding of the thermal-hydraulic details, and the development of reliable constitutive relations for periodic flow in various components of PTRs are among the areas in need of research.

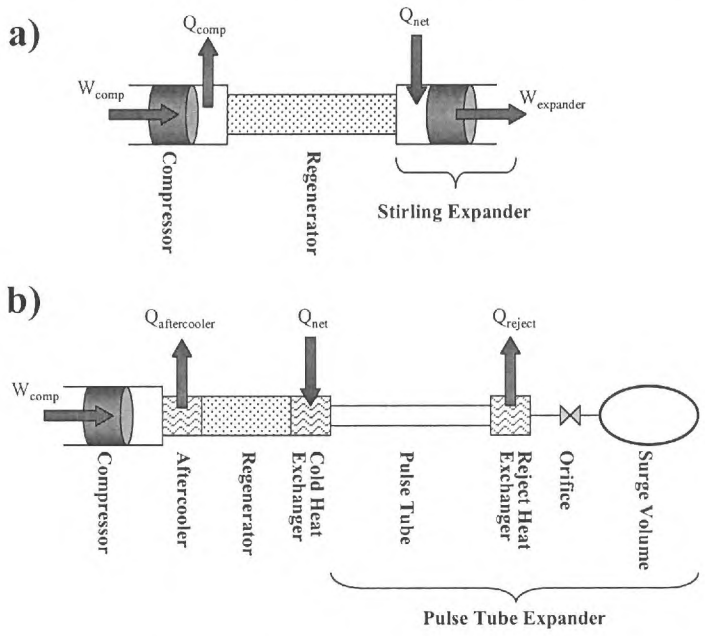

Figure 1.1. Schematic diagrams of Stirling Cycle (a) and Pulse Tube (b) cryocoolers.

Miniaturization of Pulse Tube Cryocoolers

Miniaturization of PTRs will facilitate their application in systems where low weight is essential and space for cryocooling components is limited, and is thus of great interest.

The past and current design and analysis methods and tools that are available for large Stirling machines and PTRs are unlikely to be directly applicable to their miniature counterparts without at least some major modifications, however.

Excluding the compressor, generally speaking several conditions must be met for a cryocooler system to perform effectively. These conditions are:

1. Axial (longitudinal) temperature stratification
2. Strong regeneration with reasonably low pressure drop
3. Near plug flow regime in the pulse tube
4. Small losses
5. Efficient cold and warm end heat exchangers
6. Good flow control (valves, orifices, etc.) and phase shift mechanism (orifice, inertance tube, etc.)

Among the above conditions, the first three are absolutely essential. The remainder is also important for the efficiency of the cryocooler system.

Several issues, all resulting from physical scale reduction, contribute to the difference between miniature and large PTRs. Among them are:

a. Surface friction, and heat gain/loss. The surface-to-volume ratio increases with the reduction of the physical scale, rendering surface effects more prominent in miniature PTRs. Parasitic losses due to viscous dissipation are thus likely to be more significant in miniature cryocoolers.
b. Thermal effects caused by large temperature gradients in miniature cryocoolers. Strong axial heat conduction in the solid structures may provide for direct heat transfer between hot and cold ends of the pulse tube (PT), leading to the deterioration of the PTR performance parameters. The solid structures that can contribute to adverse heat conduction include the pulse tube as well as the porous matrix of the regenerator. An additional effect is

the longitudinal conduction in the working fluid. Longitudinal conduction is often neglected in common flow situations, since it is insignificant in comparison with conduction in the fluid in other directions. The neglect of longitudinal conduction in fact is part of the classical boundary layer theory. In meso and micro scales, however, the longitudinal fluid conduction can be significant. It has in fact been demonstrated that the neglect of heat transfer in solid vessels and the working fluids can cause misinterpretation of experimental data (Herwig and Hausner, 2003, Tiselj et al., 2004).

c. Periodic flow in miniature components. For the PTR to function, the thermal boundary layers that form periodically must remain thin in comparison with component diameters. It is also necessary that periodic gas displacements be small in comparison with the component lengths, otherwise warm fluid will directly penetrate the cold end of the cooler in each period. These restrictions will require high frequency operation for miniature PTRs, and may also require larger length-to-diameter ratios in miniature PTRs.

d. The effect of connecting capillaries and micro channels. The total passive (dead) volume of these components, in comparison with the volume of the essential PTR components, is likely to be considerably larger in miniature PTRs. The extra thermal inertia associated with the connecting capillaries and their fluid contents is deleterious to the efficiency of miniaturized cryocoolers.

e. Flow in the regenerator. In comparison with large PTRs, miniature PTRs are likely to have larger pore characteristic size/regenerator diameter ratios. Preferential flows through unblocked near-wall gaps, where the hydraulic resistance is considerably lower than elsewhere in the regenerator, will also be more significant in miniature PTRs. These preferential flows can contribute to the formation of an internal flow loop of un-regenerated fluid, a phenomenon known as direct current (DC) flow, and cause thermal instability (Waldauf, Thurke, and Seidel, 2004, and Liang, et al., 2000). As devices scale down to meso and micro size range, the regenerators may need to be fabricated using MEMS or even Nano techniques. Currently, MEMS and

Nano fabrication is perfectly feasible for small scale regenerators; however, the big question is the performance of these regenerators. Pressure drop and heat transfer in micro scale regenerator structures could be different than in macro scale regenerators.

f. The performance of phase shift mechanisms (orifice, inertance tube, etc.). The phase shift mechanisms can have an important impact on the performance of PTRs. In meso scale, and particularly in micro scale, the pressure losses, and even the possible occurrence of velocity slip at the fluid-solid interphase, should be considered.

The above attributes of miniature PTRs need careful consideration and analysis since they may result in performance deterioration as the PTR size is reduced. This type of analysis is not straightforward, however, due to the strong coupling among the multitude of phenomena that result from physical scale reduction.

Small PTRs, with PT diameters as low as 0.5 cm, have been built and discussed in the open literature in the recent past (e.g., Liang, et al., 2000, Xu, et al., 1996, Tward, et al., 1999, and Nika, et al., 2004). However, these PTRs do not qualify as meso or micro systems as defined for this proposed research (i.e., less than 0.5 and 0.05 mW of exergetic cooling for meso and micro scales, respectively). An experimental investigation involving a micro-scale PTR system manufactured using MEMS technology has been reported recently (Nika, et al., 2004). Their system was designed for microelectronic cooling, however, and its demonstrated operating parameters for their system do not fall in the cryogenics range. To date no systematic study of PTR cryocoolers in the aforementioned meso or micro scales have been reported in the open literature.

The present research program has sought to remedy this situation through the development of both numerical and experimental tools to analyze and optimize small-scale PTRs. Several key task groups have been performed in parallel toward this goal. First, general scoping of the design scales and operating parameters for miniature

cryocoolers has been performed using the existing SAGE modeling code to provide a baseline for development. Second, CFD-based models using the FLUENT software package have been developed focusing specifically on the challenges for small-scale operation as described above. Third, closure relationships have been experimentally determined for the mesh filler materials for both the regenerator and heat exchanger elements within the system which for small-scale operation require denser mesh screen than for conventional units. Fourth, full CFD simulations of the miniature cryocooler operation at both meso- and micro-scales are performed for direct comparison to the earlier SAGE results and to provide more accurate tools for design setting and optimization [with full results for these to be included in the final report]. Finally, manufacturing analysis has been performed considering the appropriate materials and fabrication techniques to create the various PTR elements, including the fabrication of a meso-scale PTR which will be tested to provide experimental data for validation of the CFD simulations [with results to be included in the final report]. Basic information regarding the research methodology, assumptions, and procedures is provided in Section 2, with results from each of the task groups presented in Section 3. Finally, conclusions from the present research and recommendations for future research and development are presented in Sections 4 and 5, respectively.

2. METHODS, ASSUMPTIONS, AND PROCEDURES

2.1 Remarks about Modeling of Miniature Cryocoolers

Modeling and analysis of miniature PTRs needs to be done with caution, because some of the phenomena affecting their performance are likely to differ from those that are dominant at larger scales. As a result, the applicability of currently existing analytical tools for the design of miniature PTRs is uncertain. Even the most advanced PTR design tools [Gideon 1999, Yu 1998] are typically one-dimensional and rely on constitutive and closure relations that are at best crude approximations for the complex and periodic flow conditions in PTRs. As PTRs are miniaturized, it is expected that multi-dimensional flow effects and detailed prediction of thermal-hydraulic flow phenomena, particularly in the regenerator, will become even more important, requiring models able to accurately represent these flow details. Recent successful CFD models of cryocooler systems using Fluent [Cha, J.S., Ghiaasiaan, S.M., Desai, P.V., Harvey, J.P., and Kirkconnel, C.S., "Multi-Dimensional Effects in Pulse Tube Refrigerator", Cryogenics, 658-665, 2006] have shown that such models can provide useful performance predictions for pulse tube refrigerators. Fluent is a state of the art commercial CFD package capable of detailed solutions of models encompassing very complex geometries in two or three dimensions. It is capable of obtaining either steady state or transient solutions to problems involving a variety of flow phenomena, including flow in porous media. Fluent may also be expanded using user defined functions (UDFs) in order to add or modify closure relations and incorporate custom boundary conditions.

Because CFD models such as Fluent solve the governing conservation equations throughout the model domain, they do not include simplifying approximations and assumptions which are present in dedicated PTR models, and therefore there may be more confidence about their applicability to miniature systems. CFD models are also able to predict the complex flow details overlooked by other 1-D models, likely improving their accuracy for miniature PTRs. For these reasons, CFD modeling is likely to be the best available technique for modeling miniature PTR's. It must be emphasized, however, that experiments will be needed at some stage to verify the simulation results.

There are a few limitations, however, that come along with the advantages of CFD modeling. The models still need accurate closure relations and boundary conditions in order to produce meaningful results, particularly with regard to the hydrodynamic and thermal transport processes occurring in the porous segments of the PTR system. To address this need, experimental measurements of the hydrodynamic parameters of stacked 635 mesh stainless steel and 325 mesh phosphor-bronze screens, materials suitable for use as regenerator and heat exchanger fillers respectively, are included in this study. Another limitation of CFD models is that their increased detail is paid for with greatly increased computational time, and thus detailed and extensive parametric studies or multi-parameter optimizations with CFD models may be prohibitively time consuming. At the outset of this investigation, such parametric studies and optimizations were necessary to produce viable miniature PTR models. Previous efforts aimed at modeling miniature PTRs in Fluent by directly scaling down larger models resulted in drastically reduced performance [Jeesung Cha, 2007] and thus the various component dimensions and operating parameters of the PTR models required preliminary optimization as the overall system size was reduced. Such optimization would be time prohibitive in Fluent; therefore, the Sage PTR modeling program was used instead to provide a rough estimate of feasible geometry and operating conditions for the miniature PTRs.

Sage is a very widely used cryocooler model and design tool incorporating component level models which can be assembled to represent almost any Stirling or pulse tube cryocooler system. It is capable of very quickly solving for the steady-periodic performance of PTR's and performing multidimensional optimization of the many input variables to its component models. Sage is limited, however, in that it cannot solve for time-dependent behavior. It is also one-dimensional, although it does include empirical corrections for some specific multi-dimensional effects. For larger scale systems Sage has proven to be rather accurate, particularly when its empirical corrections are based on directly relevant experimental results. Its direct applicability to miniature systems is unknown, however, as Sage does not include corrections for many of the phenomena expected to dominate PTR performance at the miniature scale.

To take advantage of the complimentary strengths of Fluent and Sage, the two were used in parallel to model the miniature PTRs. Thus, time could be saved in the initial model development by using Sage to perform necessary scoping, parametric and optimization studies. Fluent could then be used to authenticate and extend the results of Sage. In what follows, the Sage modeling results are presented in Section 3.2, followed by the discussion of Fluent models. CFD (Fluent) simulations will be discussed in Section 3.5, however, after the discussion of mesh filler characterization.

2.2 Scoping, Design, and Optimization with Sage

In order to facilitate parametric optimization of individual component dimensions and PTR operating conditions without requiring a prohibitive amount of computational time, the initial scaling analysis and geometry optimization for the miniature PTR models was performed with Sage. Meso and micro-scale inertance tube and novel reservoir-less [garaway and Grossman, 2007] inertance tube PTRs, shown schematically in Figure 2.2.1, were initially modeled in Sage by scaling down an existing, experimentally correlated model of a relatively small PTR. These models have approximate total volumes of 3 to 4 cubic centimeters (meso-scale) and 1 cubic centimeter (micro-scale), excluding the compressor. To arrive at the initial set of dimensions and operating conditions chosen for the Fluent models, several rounds of parameter optimizations and mapping studies were done. For conciseness, only results from the final set of models are presented in section 3.1 of this report, however. It is important to note that these Sage predictions are intended to provide an estimate of the optimal system parameters, with additional optimization to be performed in Fluent, and eventually verified by experimentation.

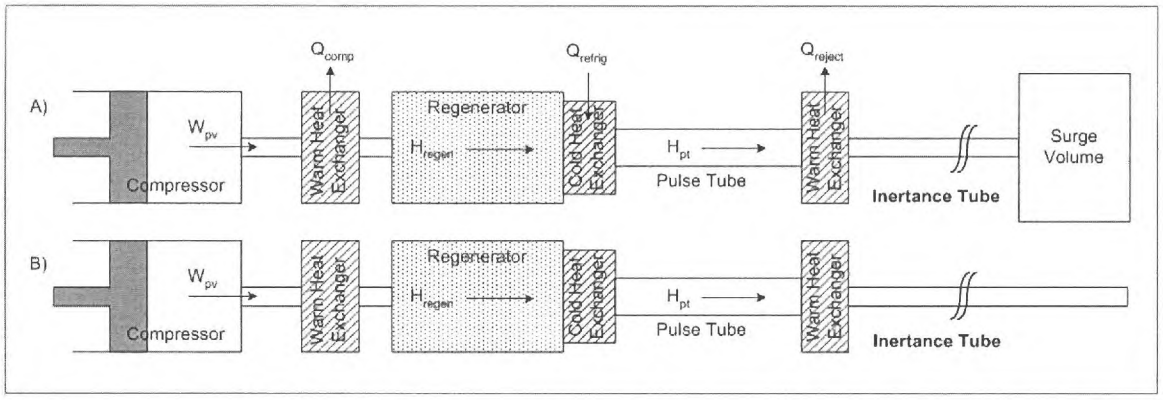

Figure 2.2.1. PTR schematics. A) Inertance Tube PTR, B) Reservoirless Inertance Tube PTR.

Even with the multi-parameter optimization capabilities of Sage, only a limited number of geometrical dimensions could be effectively optimized. Therefore, the sizes of some PTR components were fixed after scaling; this was done for the cold and warm heat exchangers and transfer lines. These dimensions were not necessarily the exact scaled values from the larger model, but rather were adjusted as necessary to ensure that they were reasonable for a practically constructible device. The pulse tube and regenerator had their diameters fixed but their lengths optimized, as did the inertance tube. When present, the volume of the reservoir was optimized as well. The compressor proved to be more difficult to scale. If its volume and stroke were optimized, Sage tended to increase them until an unrealistic pressure ratio, defined as the maximum pressure divided by the minimum pressure during a cycle, was reached. Instead, the compressor volume and piston stroke were adjusted to give a pressure ratio of 1.15 for all of the models, which was chosen to approximate the highest pressure ratio likely to be achievable with the compressor currently on our test bench. Along with the system geometry, PTR operating conditions were scaled and optimized with Sage. Particularly, the operating frequency and mean pressure were optimized in Sage, with final values chosen based upon both the Sage results and practical considerations.

2.3 CFD System-Level Modeling

As previously discussed, CFD modeling is likely to be the most accurate technique for predicting the performance of miniature PTRs. The Fluent system-level models developed in this study had their initial geometry and operating conditions based on the

Sage results discussed in section 3.1. These Sage results were not expected to produce the best possible Fluent PTR model performance, however, but were instead intended to be more of a rough estimate and starting point. Therefore, subsequent optimization of the PTR geometry will be performed using Fluent, particularly with respect to the length of the inertance tube which causes the phase shifting.

The system-level CFD models simulated here were axisymmetric, two-dimensional models utilizing second order upwind discretization, PISO pressure-velocity coupling, and a second order implicit unsteady solver. Ideal helium was used as the working fluid. Convergence criteria were set at 10^{-7} for continuity and velocity and 10^{-8} for energy. Time steps of 10 and 20 μs were used for the micro-scale and meso-scale cases, respectively, which operated at 200 and 400 Hz. For all of the cases, this resulted in 250 time steps per period of pressure oscillations.

To reduce computational time, the system-level Fluent models were started with assumed linear temperature distributions having cold temperatures as near as possible to their expected final steady state values. To set up the linear temperature distributions, models were first initialized at a constant temperature of 293 K. The warm heat exchanger exterior walls were prescribed their normal boundary conditions, a constant temperature of 293 K, while the cold heat exchanger exterior wall boundary condition was changed from adiabatic to a constant temperature, the assumed cold tip temperature. The model was then iterated using the steady state solver and conduction was allowed to set up linear temperature gradients in the pulse tube and regenerator. The cold heat exchanger exterior wall was then returned to an adiabatic boundary condition and the unsteady solver was selected to begin the simulations.

To avoid starting the models with cold temperatures too far from their final steady state cold tip temperatures, a bracketing method has been developed. Simulations are accordingly started with an assumed cold temperature and allowed to run for a short time. If Fluent predicts that the model would cool, the assumed initial cold end temperature is reduced and the model is restarted. Eventually, the model would be started at

temperatures on either side of the steady state cold temperature, bracketing it and allowing better guesses to be made. With this approach, the computational time required to reach a periodic steady state solution will be drastically reduced.

Once periodic steady state is reached, the Fluent models can be optimized by changing operating parameters in small steps or component geometries, reinitializing if necessary to the previous cold temperature, and iterating until a new periodic steady state solution was reached. These simulations are expected to reach steady periodic state rapidly, since they start from nearly periodic steady conditions to begin with.

Scoping simulations, and preliminary simulations aimed at testing various aspects of the Fluent CFD package in relation to PTR modeling have been performed. Currently, the final system-level model simulations have been started using the hydrodynamic closure parameters for 400 mesh [Cha 2007] because they were the most relevant available closure parameters. However, as part of this investigation experiments were performed to determine the hydrodynamic parameters of stacked screens of stainless steel 635 mesh and phosphor-bronze 325 mesh, materials that are more suitable for miniature PTR regenerators and heat exchangers. The methodology and results of these experiments are detailed in the forthcoming sections. Given that these results have now become available, the closure parameters representing these materials have been incorporated into the CFD models. The CFD simulations with refined closure relations will take several days, however. Since these parameters were not available at the time of preparation of this report, however, the CFD model results presented here in Section 3.3 will be based on the aforementioned 400 mesh screen closure parameters.

2.4 Mesh Filler Characterization

Accurate CFD modeling of pulse tube refrigerators requires realistic closure relations, particularly with respect to the hydrodynamic and thermal transport processes for the porous media which make up their heat exchangers and regenerators. Useful experimental data and correlations have been published recently for some widely used regenerator fillers [Cha 2007; Cha et al., 2008]. These fillers, however, may not be

appropriate for miniature cryocoolers due to their relatively coarse structure. Therefore, experimental measurements were performed to determine the hydrodynamic parameters of stacked screens of stainless steel 635 mesh and phosphor bronze 325 mesh, materials among the finest commercially available regenerator fillers and suitable for use in miniature cryocoolers.

It should be emphasized that without direct pore-level simulation, the macroscopic conservation equations which govern fluid flow through the porous media require empirical data. These relationships include the Darcy permeability and Forchheimer's inertial coefficient which are needed for the closure of macroscopic momentum conservation equation. Generally, the porous media that are encountered in regenerators are morphologically anisotropic, and thus the parameters which characterize them are anisotropic as well. Measurement of the hydrodynamic parameters in at least two dimensions is therefore preferred. Hydrodynamic parameters are also varied when these fillers are subjected to dissimilar flow fields; consequently resistance parameters were also found for steady state and steady periodic flow conditions. The directional hydrodynamic flow resistance parameters are determined here using experimental measurements of the fluid mass flow rate and the pressure drop across the porous media. By simulating the experimental test sections in CFD we can iteratively solve for unique viscous and inertial flow resistances until agreement is reached between simulated and experimental results.

The hydrodynamic parameters of stacked discs of 635 mesh stainless steel wire cloth and 325 mesh phosphor bronze wire cloth were thus experimentally measured, following the procedures to be described in the forthcoming subsections. These wire cloths are among the suitable structures for use as miniature regenerator and heat exchanger fillers. Wire cloth material was supplied from TWP Inc. and test samples were machined by Virtual AeroSurface Technologies. Measurements were made in the axial and radial directions for both steady state and steady periodic flow conditions. Higher frequency operation is preferred for miniature cryocoolers, therefore a frequency range between 50 and 200 Hz was investigated for the oscillatory flow cases. Research grade helium with a nominal

purity of 99.9999% was used in each test as the working fluid. In the following sections, the experimental and computational methodologies employed in solving for each of the hydrodynamic flow resistances are explained.

Steady Axial Flow Test Methodology

The experimental setup for determining the hydrodynamic steady, axial flow resistance parameters consisted of a helium supply tank, two Paine Electronics low pressure series 210-10 static pressure transducers, a Sierra Instruments 820 Series Top-Trak mass flow meter, a specially designed test section containing the porous sample and the associated piping and Swagelok fittings and valves. A diagram of this setup is shown below in Fig. (2.4.1).

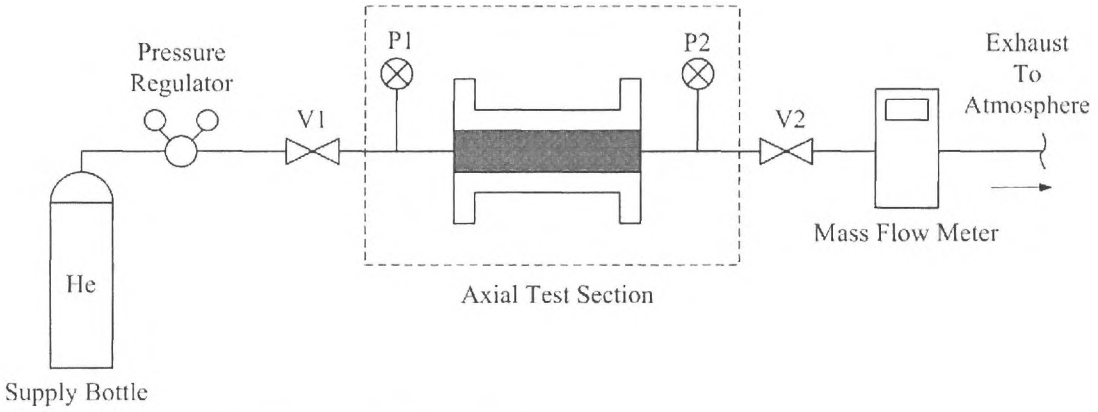

Figure 2.4.1: Axial Steady Flow Test Setup.

The steady axial flow test section is a hollow aluminum cylinder with flanged ends. Its purpose is to house the porous media or stacks of wire screens. The base pieces adjoined on either side of the axial test section help to constrain the porous samples and provide a mount for one of the static pressure transducers. Valves, V1 and V2 and the static pressure transducers, P1 and P2 are respectively located upstream and downstream of the test section.

The axial test sample was specifically designed with a high aspect ratio so that flow in the radial direction would be negligible compared with that of the axial direction. Important

characteristics of the axial porous samples included in both the steady and unsteady flow regimes (unsteady flow regime data will be discussed later) are summarized in Table 2.4.1 below. An additional axial flow sample (400 mesh stainless steel) is included in the table for comparison.

	Sample Geometry		Mesh Geometry		Measured
Porous Media	Dia mm	Length mm	Wire Dia micron	Pore Size micron	Porosity
325 Phosphor Bronze	4.0	12.7	35.6	43	0.6738
635 Stainless Steel	4.0	12.7	20.3	20	0.6312
400 Stainless Steel*	7.94	38.1	25.4	33	0.692

Table 2.4.1: Steady and Periodic Axial Flow Axial Test Sample Details
*400 Stainless Steel Sample dimensions and porosity [Cha 2007]

During each steady axial flow test, helium flows from the charged bottle through the pressure regulator, into axial test section and mass flow meter and is exhausted to the atmosphere. Each test run was performed only after strict assurance of a hermetically sealed setup. With valve V2 closed and valve V1 open, the isolated system was charged to a supply pressure of 400 psig (2.86 MPa). Valve V2 was then modulated to offer a range of mass flow rates up to 0.91 g/s. Static pressures P1 and P2 were recorded for each distinct flow rate. In order to prevent the mean pressure from varying too much over the test run the maximum allowable axial pressure drop across the test section was limited to 100 psi (0.69 MPa). Axial pressure drops were then plotted against mass flow rate and these experimental data were curved fitted to a 5^{th} order polynomial with a zero intercept in order to simplify the data analysis.

Representative experimental data points covering the full range of mass flow rates were then simulated with the Fluent CFD code. The Fluent code incorporated a 2D axisymmetric mesh that modeled the geometry of the experimental test setup from P1 to P2. Although turbulent flow was not expected in the porous section of the model,

Reynolds numbers in the open sections suggested turbulent flow and therefore the Reynold's-Averaged Navier-Stokes, k-epsilon, turbulent flow model was used. A single Fluent case was created for each representative data point and experimentally-measured parameter values were input as boundary conditions for simulations. A mass flow rate boundary condition was used at the inlet while a pressure outlet boundary condition was implemented downstream at the P2 location. The model's viscous and inertial resistances were iteratively changed until there was agreement between the simulated area-weighted static pressure at the inlet and experimental static pressure at P1 at all chosen data points. Results for the steady axial flow test sample characterization are shown in section 3.4.2.

Oscillatory Axial Flow Test Methodology

The periodic, axial flow experimental setup consisted of a Hughes Aircraft Tactical Condor compressor, HP-Agilent 33120A function waveform generator and HP-Agilent 3852A data acquisition control unit, Crown DC-300A Series II amplifier, two constant-temperature hot wire anemometers with TSI Flowpoint 1500 Series signal conditioner, two high frequency PCB Piezotronics 101A05 dynamic pressure transducers, a specially designed test section containing porous media and the associated piping, fittings and helium charge tank. An HP VEE virtual console was operated to integrate all sensor data. A diagram of the periodic flow axial setup is shown below in Fig. 2.4.2.

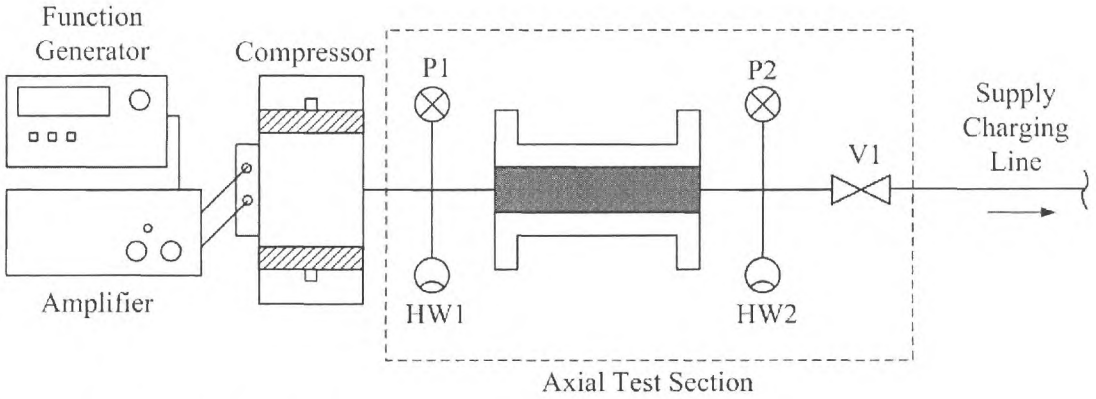

Figure 2.4.2: Axial Periodic Flow Test Setup.

The experimental setup for periodic, axial flow is a closed system bounded by the compressor and the valve, V1. The oscillatory flow axial test section consists of the same

hollow aluminum cylinder utilized in the steady flow axial setup. It houses the 4 mm diameter stack of discs but is coupled with a different set of sensor mounts attached on either side of it. On the side adjoining the compressor there is a base piece which contains a dynamic pressure transducer, P1, accompanied with a hot wire probe, HW1. The opposite base piece contains another dynamic pressure transducer, P2, as well as another hot wire probe, HW2. Both sensor mounts are also internally fitted with an 8.0 degree sloped transition cone located between the cylindrical porous test section and sensor tap locations. This transition avoids a large step change in pipe diameter and acts to reduce flow disturbance, improving the hot wire signal.

For each unsteady axial test run the system is leak tested and charged. A sinusoidal signal sent to the compressor is amplified to provide the largest stable pressure oscillation at each frequency. Waveforms from the hotwires are directly recorded to compare with the Fluent model results, while the periodic pressures are represented by their first three harmonics, calculated using an FFT. Data was taken at seven distinct frequencies from 50 to 200 Hz in intervals of 25 Hz at operating pressures of approximately 400 psig (2.86 MPa) and 490 psig (3.38 MPa). It is under these conditions of high charge pressures and higher operating frequencies that we expect the miniature PTR to function.

A 2D axisymmetric mesh models the experimental test section geometry between P1 and valve V1, and the associated Fluent simulation employs a laminar flow regime. A user defined oscillatory pressure inlet boundary condition is implemented at P1 based upon the aforementioned Fourier series representation of the experimental results. The viscous and inertial resistances of the simulation were iteratively changed until there was agreement between the simulated area-weighted static pressure at P2 and experimental static pressure at P2. The periodic flow axial hydrodynamic parameters may then be further validated by comparing experimental data from HW1 and HW2 to simulated mass flow rates, although these results are not presented here. Results for the oscillatory axial flow test sample characterization can be found in section 3.2.3.

Steady Radial Flow Test Methodology

The steady radial flow experimental setup is an open system similar to the steady axial flow test apparatus. It incorporates all of the apparatus developed in the steady flow axial test with the exception of the test section and sensor mounted base pieces. A diagram of this setup is shown below in Fig. 2.4.3.

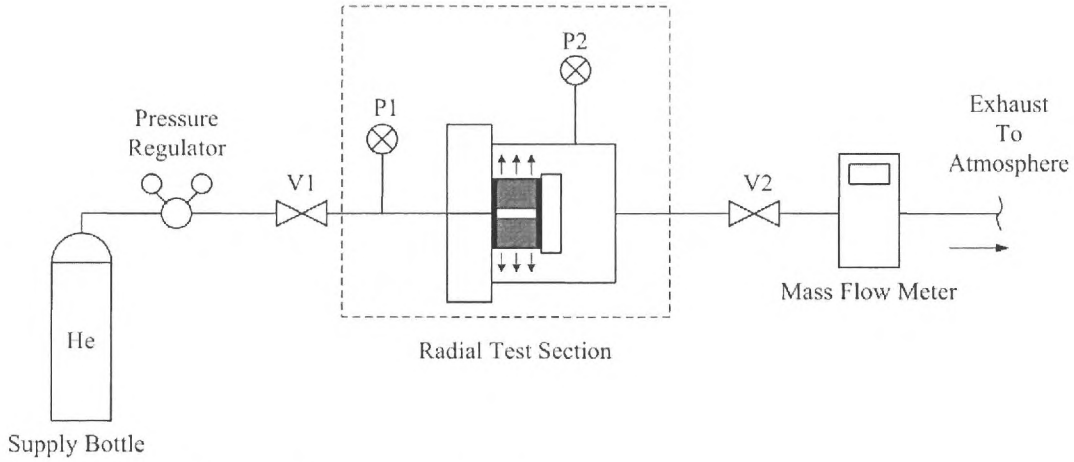

Figure 2.4.3: Radial Steady Flow Test Setup.

The radial test section contains an annular ring of porous media mounted onto an aluminum slab constrained by a cap, nuts and three threaded rods. Like the axial samples the radial test samples were specifically designed to produce a predominantly radial flow regime within the porous media. Rubber gaskets on either side of the porous material ensure that all the mass flux passes in the radial direction through outer diameter. The length of the annular porous sample is prescribed by tightening the nuts on the threaded rods to adjust the porosity of the test section to closely match its axial flow test section counterpart.

Important characteristics of the radial porous samples included in both the steady and unsteady flow regimes are summarized in Table 2.4.4 below. Parameters for an additional radial test section filler that has been previously studied are included for comparison.

	Sample Geometry			Mesh Geometry		Measured
Porous Media	I.D.	O.D.	Length	Wire Dia	Pore Size	Porosity

	mm	mm	mm	micron	Micron	
325 Phosphor Bronze	4.0	20.0	3.4	35.6	43	0.670
635 Stainless Steel	4.0	20.0	6.1	20.3	20	0.630
325 Stainless Steel*	4.0	20.0	9.53	35.6	43	0.632

Table 2.4.4: Steady and Periodic Radial Test Sample Details
*325 Stainless Steel Sample dimensions and porosity [Cha 2007]

Like the steady axial flow experimental setup, helium is supplied by a pressure regulator through the radial test section and into the mass flow meter until it is vented to the atmosphere. Static pressure transducers P1 and P2 and valves V1 and V2 are respectively located upstream and downstream of the porous test section. Once the system was leak tested, it was charged to a pressure of 400 psig (2.86 MPa). The valve V2 was then throttled to offer a range of mass flow rates up to 1.5 g/s. Static pressures, P1 and P2 were recorded for each discrete mass flow rate. Radial pressure drops were plotted against mass flow rate and experimental data was curved fitted to a second order polynomial with a zero intercept. Experimental data points selected over the entire range of mass flow rates were then simulated into the forthcoming CFD analyses.

A 2D axisymmetric CFD model was created to simulate the experimental setup geometry between P1 and P2. A steady flow Fluent simulation utilizing a laminar flow regime was created for each representative data point and empirical values were input as boundary conditions for simulations. A mass flow rate boundary condition was used at the inlet while a pressure outlet boundary condition was implemented downstream at the P2 location. The viscous and inertial resistances of the simulation were iteratively changed until there was agreement between the simulated area-weighted static pressure at the inlet and experimental static pressure at P1 for all chosen data points. Results for the steady radial flow test sample characterization are shown in section 3.2.4.

Oscillatory Radial Flow Test Methodology

The periodic radial flow experimental setup was very similar to the periodic axial flow setup. Its setup included all of the instrumentation and the data acquisition system employed in the periodic axial flow experiment with the exception of the sample test section and sensor mounting pieces. An HP VEE virtual console was again used to

integrate all sensor data. A diagram of the periodic radial flow apparatus is shown in Fig. 2.4.4.

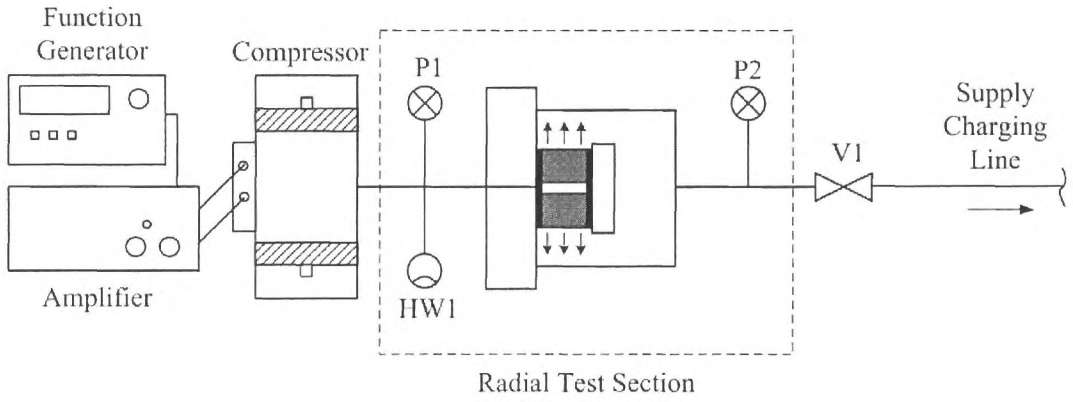

Figure 2.4.4: Radial Periodic Flow Test Setup.

The experimental setup for periodic radial flow is a closed system bounded by the compressor and the valve V1. The oscillatory radial flow test section consists of the same sample test section utilized in the steady radial flow setup. The porous media is constrained by the aluminum slab and cap with threaded rods. Rubber gaskets are placed on either side of the sample and nuts are tightened down to a specified length to match the sample porosity its steady flow counterpart. Unlike the oscillatory axial flow test setup, the high frequency dynamic pressure transducers are mounted by inline fittings. Pressure sensors P1 and P2 are respectively located on either side of the porous media. The hot wire probe, HW1, shares the same axial location in the experimental setup as P1.

For each unsteady radial test run, the system is leak tested and charged to the working pressure, and a sinusoidal waveform sent to the compressor is amplified to provide the largest stable pressure oscillation at each frequency. Again, waveforms of the measured velocity were recorded while the pressure signals were represented using the first three harmonics of an FFT. Data was taken at seven frequencies from 50 to 200 Hz in intervals of 25 Hz at operating pressures of approximately 400 psig (2.86 MPa) and 490 psig (3.38 MPa).

A 2D axisymmetric mesh simulates the experimental test section geometry between P1 and valve V1 and the associated CFD simulation employs a laminar flow regime. A user defined oscillatory pressure inlet boundary condition is implemented at P1 based upon the Fourier series representative of the experimental results. The viscous and inertial resistances of the simulation were iteratively changed until there was agreement between the simulated area-weighted static pressure at P2 and experimental static pressure at P2. The periodic radial flow hydrodynamic parameters were further validated by comparing the experimental and simulated mass flow rate at HW1. Results for the oscillatory radial flow test sample characterization can be found in section 3.2.5.

3. RESULTS AND DISCUSSION

3.1 Scoping Design and Optimization with SAGE

In order to facilitate parametric optimization of individual component dimensions and PTR operating conditions without requiring a prohibitive amount of computational time, the initial scaling analysis and geometry optimization for the miniature PTR models was performed with Sage. Meso and micro-scale inertance tube and reservoir-less inertance tube PTR models having approximate total volumes of 3 to 4 cubic centimeters (meso-scale) and 1 cubic centimeter (micro-scale), excluding the compressor were constructed in Sage. To arrive at the initial set of dimensions and operating conditions chosen for the Fluent models, several rounds of parameter optimizations and mapping studies were done with these models. For conciseness, only results from the final set of models are presented in this report.

Dimensions of several PTR components were fixed after the initial model scaling, with geometry chosen based upon practical considerations for the eventual prototype construction (See Section 3.6). These included the warm and cold heat exchangers and the transfer lines. Other components such as the pulse tube, regenerator, and inertance lines had their diameters fixed but their lengths optimized. The operating frequency and mean pressure were also optimized in Sage, with final values chosen based upon both the Sage results and practical considerations. For all the models, compressor geometry was fixed to provide a pressure ratio of 1.15 to the cold head; this value was chosen to approximate the highest pressure ratio likely to be achievable with the compressor currently on our test bench.

Sage modeling of the effects of mean pressure and operating frequency on performance for the miniature PTRs indicated that performance would increase along with either parameter, as increasing frequency or charge pressure result in higher input power to the model. In fact, the Sage optimizer would not predict reasonable upper bounds for either charge pressure or operating frequency but instead increased both without limit. Therefore, values of these parameters were chosen and the remaining model geometry

was optimized around them. The operating pressure was fixed at 3.55 MPa (515 psi), the maximum absolute pressure currently available on our test bench. The frequency was set at 200 Hz, also based on compressor restrictions.

For many of the PTR component dimensions, there was no distinct value resulting in maximal overall system performance. Often, the Sage – predicted performance asymptotically approached a maximum as component lengths increased beyond the reasonable dimensions of a miniature PTR. Thus, compromises had to be made between achieving maximum performance and limiting the overall system size. Figures 3.1.1 and 3.1.2 show the variation of the overall system performance with changes in pulse tube length and regenerator length. For each point in these figures, the compressor stroke and inertance length were optimized to provide a pressure ratio of 1.15 and optimal phase shift. For the meso-scale models, the cold tip temperature was 150 K while for the micro-scale models it was 170K. These mappings allowed the determination of the minimum component dimensions which still allowed very good system performance.

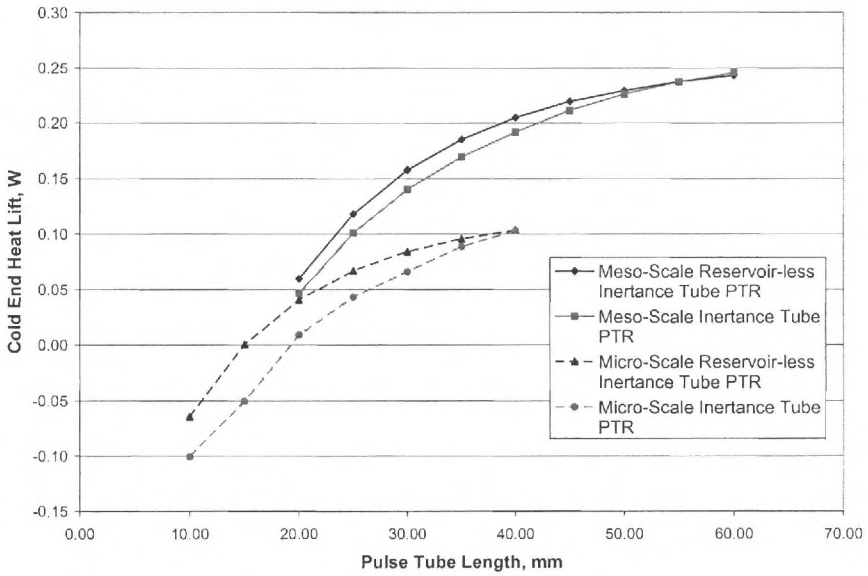

Figure 3.1.1. Predicted Performance vs. Pulse Tube Length

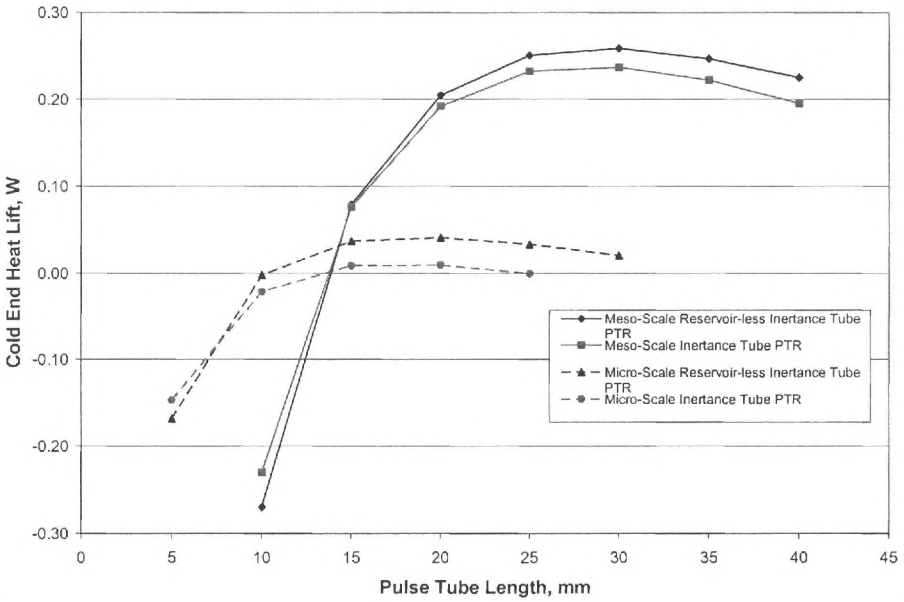

Figure 3.1.2 Predicted Performance vs. Regenerator Length

A multitude of inertance line lengths can provide near – optimal phase shift and thus maximize performance. The absolute maximum system performance occurs with the shortest of these, however, and so it is important to start the Sage optimizer near this length so that it doesn't pick up one of the other, less optimal points by mistake. The variation in system performance due to changes in the inertance tube length is shown in Figure 3.1.3 for all four models.

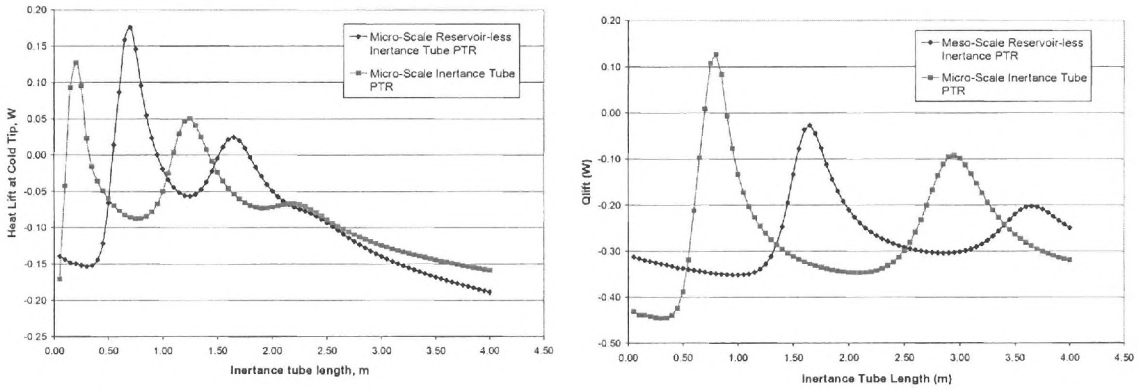

(A) (B)

Figure 3.1.3 A) Micro-Scale and B) Meso-Scale PTR performance vs. Inertance Tube Length

Figure 3.1.4 shows load curves for the meso and micro-scale models with constant pressure ratio of 1.15. At the meso-scale, Sage predicts ultimate (no-load) cold temperatures of 102 K and 104 K for the standard inertance tube and reservoir-less inertance tube PTRs, respectively. At the micro-scale, these two cooler types were predicted to reach 145 K and 144 K.

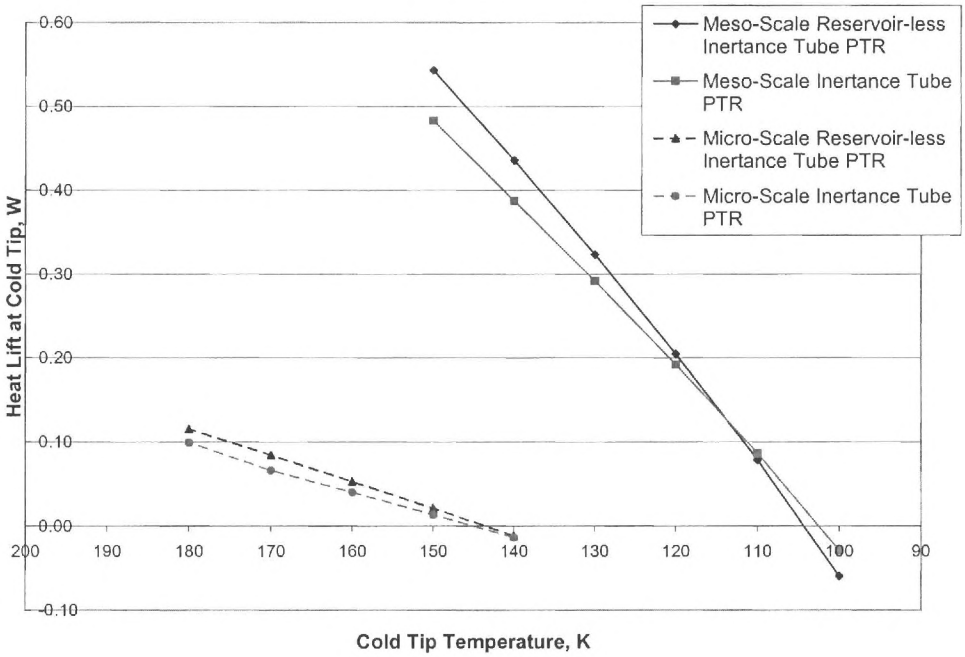

Figure 3.1.4. Load Curves for Micro-Scale and Meso-Scale Sage PTR Models

Based on these Sage modeling results, initial dimensions and operating conditions for meso-scale and micro-scale Fluent models were determined. These are given for the various models in Table 3.2.1 below. Practical considerations of device construction and available test facilities were also taken into account in their selection, as well as the desire to keep the system dimensions as small as possible.

Model	regenerator		pulse tube		inertance tube		Mean Pressure	frequency
	length (mm)	diameter (mm)	length (mm)	diameter (mm)	length (m)	diameter (mm)	(MPa)	(Hz)
Meso-Scale Inertance Tube	20	4	40	2.5	0.8097	0.6	3.55	200
Meso-Scale Reservoir-less Inertance Tube	20	4	40	2.5	1.656	0.6	3.55	200
Micro-Scale Inertance Tube	20	2	30	1	0.2176	0.4	3.55	400
Micro-Scale Reservoirless Inertance Tube	20	2	30	1	0.688	0.4	3.55	400

Model	Warm Heat Exchanger 1		Cold Heat Exchanger		Warm Heat Exchanger 2		total	(SAGE) Cold
	length (mm)	diameter (mm)	length (mm)	diameter (mm)	length (m)	diameter (mm)	volume (cc)	Temp (K)
Meso-Scale Inertance Tube	10	4	4	4	5	4	4.06	102
Meso-Scale Reservoir-less Inertance Tube	10	4	4	4	5	4	2.29	104
Micro-Scale Inertance Tube	5	2	3	2	3	2	0.9834	145
Micro-Scale Reservoirless Inertance Tube	5	2	3	2	3	2	0.2425	144

Table 3.1.1. Summary of Sage – optimized meso and micro – scale PTR dimensions.

3.2. Mesh Filler Characterization for Closure Relationships

3.2.1 General Remarks

This section describes the results of experiments and simulations performed to determine the hydrodynamic parameters of the 635 stainless steel and 325 phosphor bronze wire mesh samples. Utilizing a unique experimental test setup for each specified direction and flow regime, measurements were made in the axial and radial directions for both steady state and steady periodic flow conditions. All periodic measurements were done at the largest stable input pressure based upon compressor response. Oscillatory flow parameters in the axial and radial directions were applied to a range of operating frequencies between 50 and 200 Hz at charge pressures of 400 psig (2.76 MPa) and 490 psig (3.38 MPa).

3.2.2 Steady Axial Flow

The results for the steady axial flow hydrodynamic characteristics are presented in this section. A supply pressure of 400 psig (2.78 MPa) was utilized for each steady axial flow test run. A plot of experimental and simulated steady flow axial pressure drops and mass flow rates for both test samples are displayed below in Fig. 3.2.2.

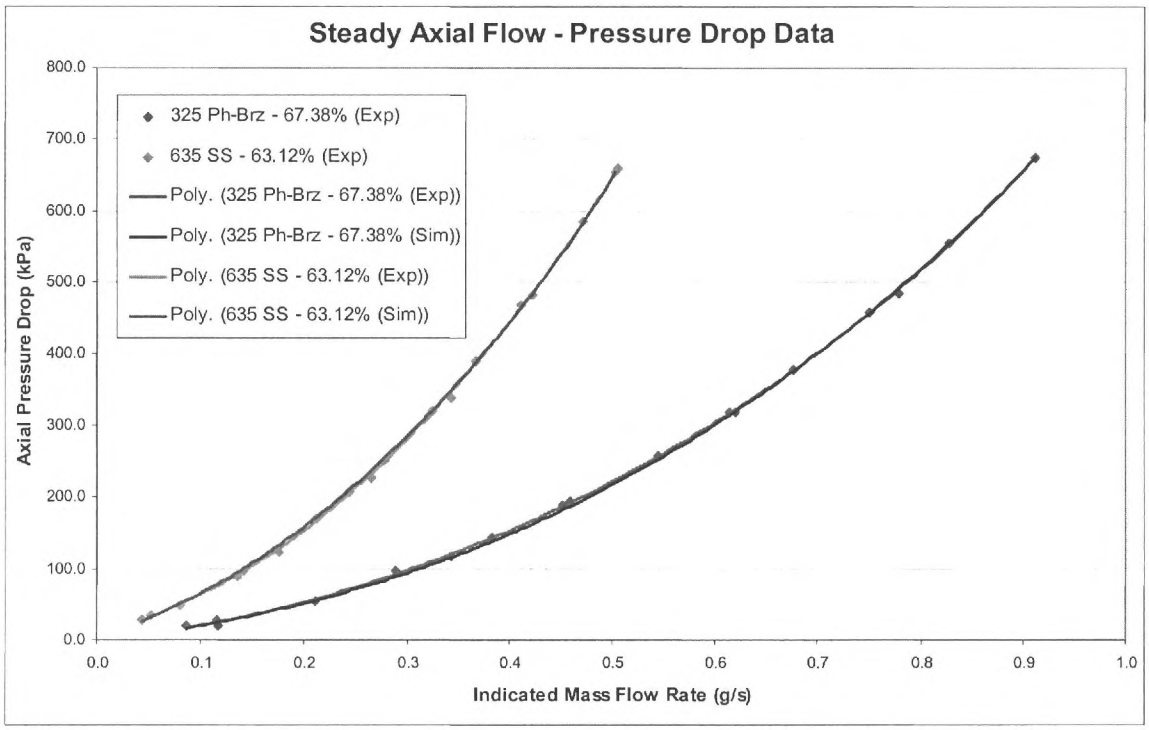

Figure 3.2.1: Steady axial flow pressure drop plots for 325 phosphor bronze and 635 stainless steel samples

Good agreement is displayed between experimental and simulated data over the entire range of flow rates. Due to the small cross sectional area of the steady axial flow test sample housing large pressure drops were recorded. This pressure drop as mentioned before was limited to a maximum axial pressure difference of 100 psi (0.689 MPa) offering a maximum mass flow rate of only 0.9 g/s for the more porous, 325 phosphor bronze mesh sample. A summary of the results for the steady flow axial hydrodynamic resistances and Darcy permeability and Forchheimer's coefficients are provided in Table 3.2.1 below. Parameters from an additional mesh sample that was previously studied by Cha (2007) are included for comparison.

Porous Media	Viscous Resistance 1/m^2	Inertial Resistance 1/m	Darcy Permeability m^2	Forchheimer's Coefficient ---
325 Phosphor Bronze	2.85E+10	28000	1.593E-11	0.183
635 Stainless Steel	9.95E+10	65000	4.004E-12	0.259

400 Stainless Steel*	2.77E+10	73000	1.753E-11	0.452

Table 3.2.1: Steady flow axial sample hydrodynamic parameters
*400 Stainless Steel Parameters [Cha 2007]

3.2.3 Oscillatory Axial Flow

The results for the oscillatory axial flow hydrodynamic characteristics are presented in this section. A specific methodology is used to find the unique oscillatory parameters for each porous material. The viscous resistance term is iteratively solved for first at low flow conditions where input pressure amplitudes are just large enough for a viable signal. Flow in this regime can be considered to be purely Darcy flow, where only viscous effects are significant and inertial effects are negligible. Only the viscous resistance term is then iteratively solved for at these low flow conditions while the inertial resistance is fixed at zero. An application of this process is shown below in Fig 3.2.2 for the low flow stainless steel 635 mesh filler at 50 Hz at 490 psig (3.38 MPa).

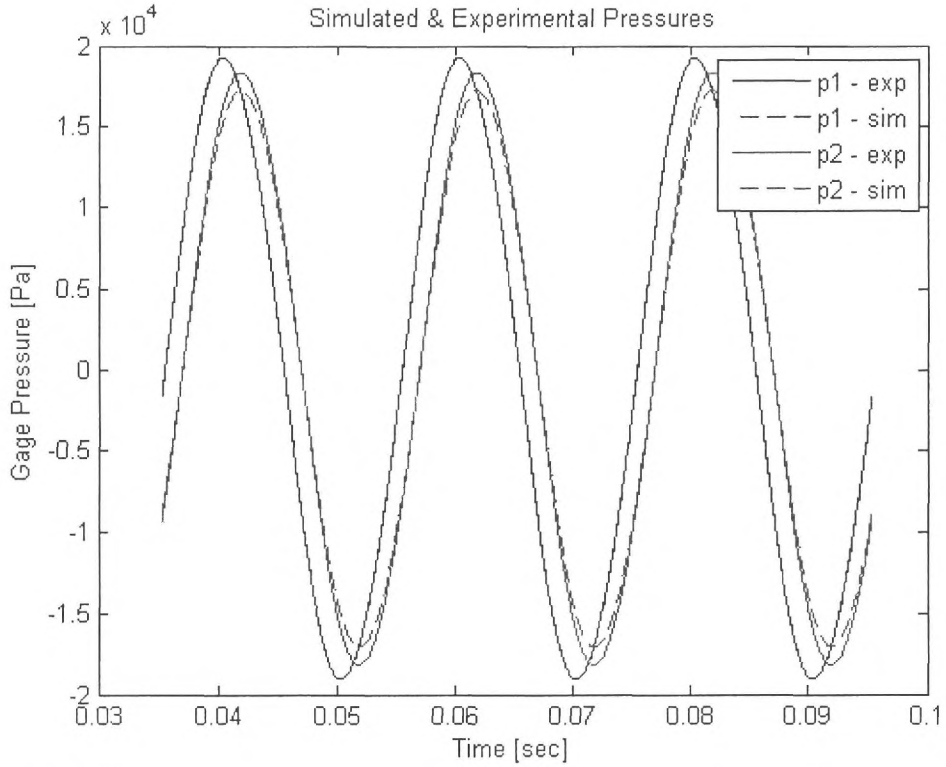

Figure 3.2.2: 635 stainless steel experimental and simulated periodic axial flow pressure plots at 50 Hz low flow conditions (490 psig)

In Figure 3.22 it is clear that the experimental and simulated pressure signals at P1, which are identical, are lagged by the two signals at P2. Although the amplitudes of the experimental and simulated data representing pressure at P2 are not exact the same, the phase shifts relative to P1 are nearly identical. Once the experimental and simulated phase shifts and pressure amplitudes at P2 are in accord, the viscous term is then set and the inertial term can be solved for at higher flow conditions. Slight adjustments to the viscous term were made to obtain better agreement for higher flow cases. A plot of the experimental and simulated pressures at P2 for the 635 mesh at 490 psig (3.38 MPa) and 150 Hz are shown in Fig. 3.2.3.

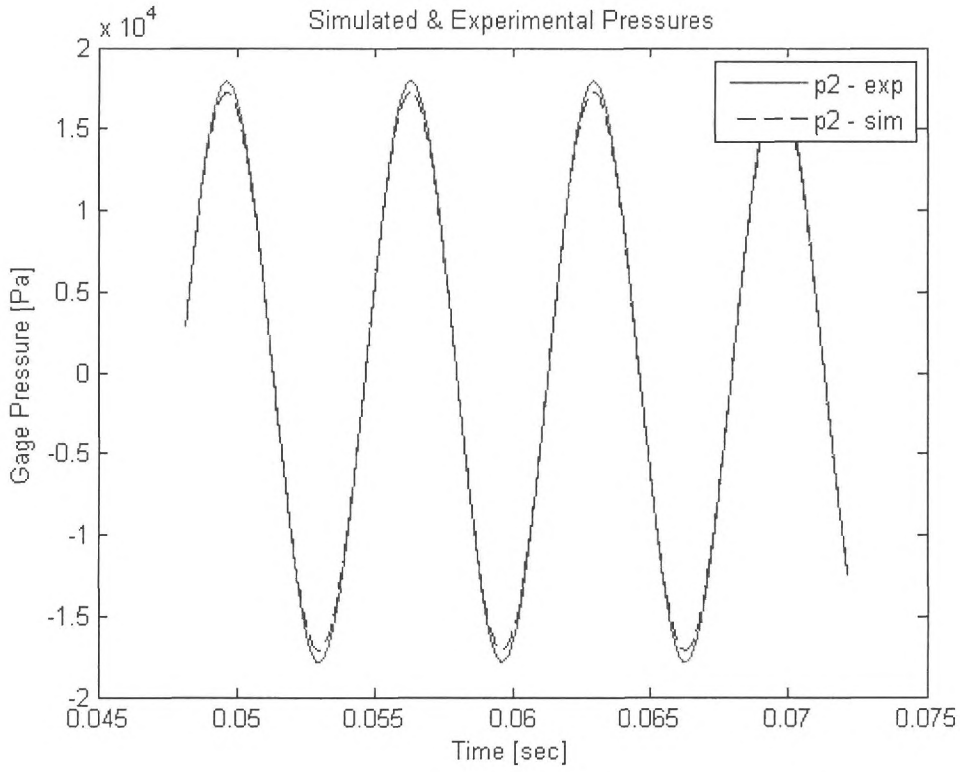

Figure 3.2.3: 635 stainless steel experimental and simulated periodic axial flow pressure plots for at 150 Hz (490 psig).

The iterative solution method produced a unique set of axial flow parameters for each test sample at each charge pressure. Results for the oscillatory flow axial hydrodynamic resistances and Darcy permeability and Forchheimer's coefficients are summarized in Table 3.2.2.

Porous Media	Charge Pressure psig	Viscous Resistance 1/m^2	Inertial Resistance 1/m	Darcy Permeability m^2	Forchheimer's Coefficient ---
325 Phosphor Bronze	400	1.70E+10	50000	2.672E-11	0.422
325 Phosphor Bronze	490	1.70E+10	50000	2.672E-11	0.422
635 Stainless Steel	400	9.50E+10	40000	4.194E-12	0.163
635 Stainless Steel	490	9.50E+10	40000	4.194E-12	0.163
400 Stainless Steel*	400	3.95E+10	120000	1.211E-11	0.630

Table 3.2.2: Periodic flow axial sample hydrodynamic parameters.
*400 Stainless Steel Parameters [Cha 2007]

3.2.4 Steady Radial Flow

Results for the steady radial hydrodynamic parameters are shown in this section. The experimentally measured pressure drops for the 325 mesh phosphor bronze and the 635 mesh stainless steel fillers are shown in Fig 3.2.4.

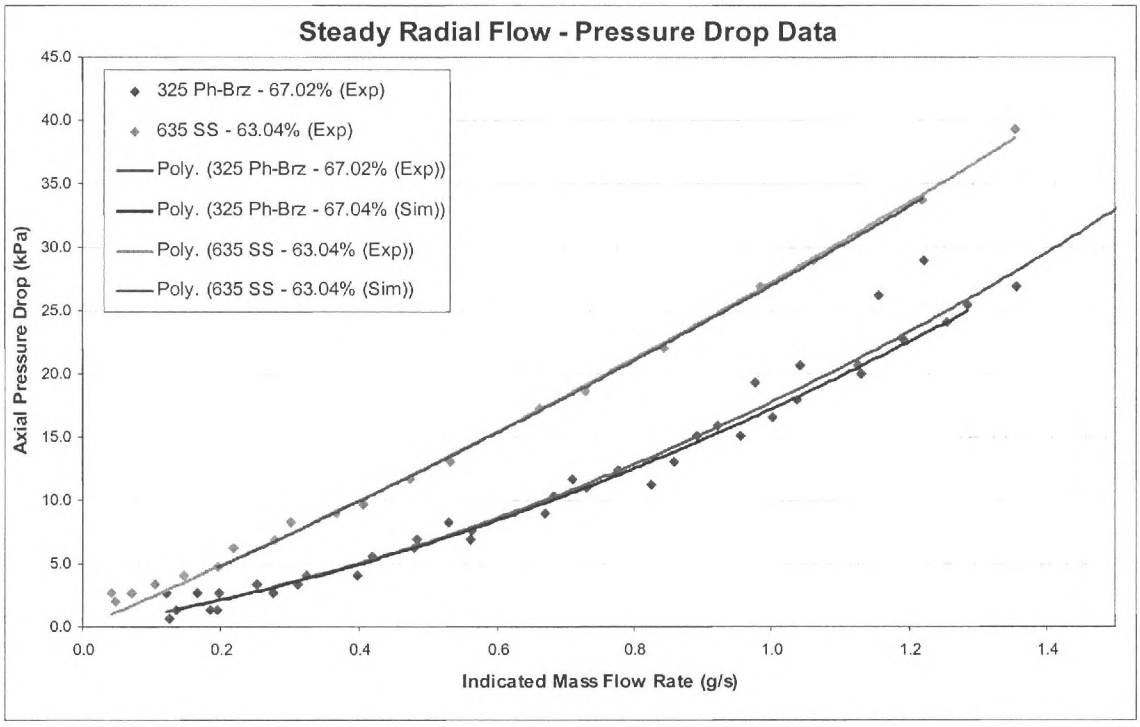

Figure 3.2.4: Steady radial flow pressure drop plots for 325 phosphor bronze and 635 stainless steel samples.

The nearly radial pressure drop plots indicate that the regime is predominately Darcy or viscous flow pattern with little inertial effects. Radial test runs produced only minor pressure drops over the specified range of mass flow rates. With only a maximum change in pressure of 40 kPa across the porous media, the observable data was approaching the instrumentation's limit of accuracy. Perhaps, by using an annular test sample with a larger outer diameter and decreased length there would be an increased pressure drop in the radial direction for a given mass flow rate providing more precise measurement. Table 3.2.3 is a summary of the hydrodynamic parameters that were determined based on these experiments.

Porous Media	Viscous Resistance 1/m^2	Inertial Resistance 1/m	Darcy Permeability m^2	Forchheimer's Coefficient ---
325 Phosphor Bronze	2.85E+10	58000	1.576E-11	0.382
635 Stainless Steel	1.24E+10	59000	3.205E-11	0.667
325 Stainless Steel*	6.80E+09	98600	7.001E-11	1.219

Table 3.2.3: Steady Flow Radial Sample Hydrodynamic Parameters
*325 Stainless Steel Parameters [Cha 2007]

3.2.5 Oscillatory Radial Flow

The characterization process for the oscillatory radial flow case is very similar in development to that of its periodic axial counterpart. The viscous term was first focused on at low flow rates. It was then affixed at the higher flow rates where the inertial resistance was then iteratively obtained. The results for the oscillatory axial flow hydrodynamic characteristics are discussed in this section. A plot of the experimental and simulated pressures at P2 for the 635 mesh at 400 psig (2.76 MPa) and 175 Hz are shown in Fig. 3.2.5.

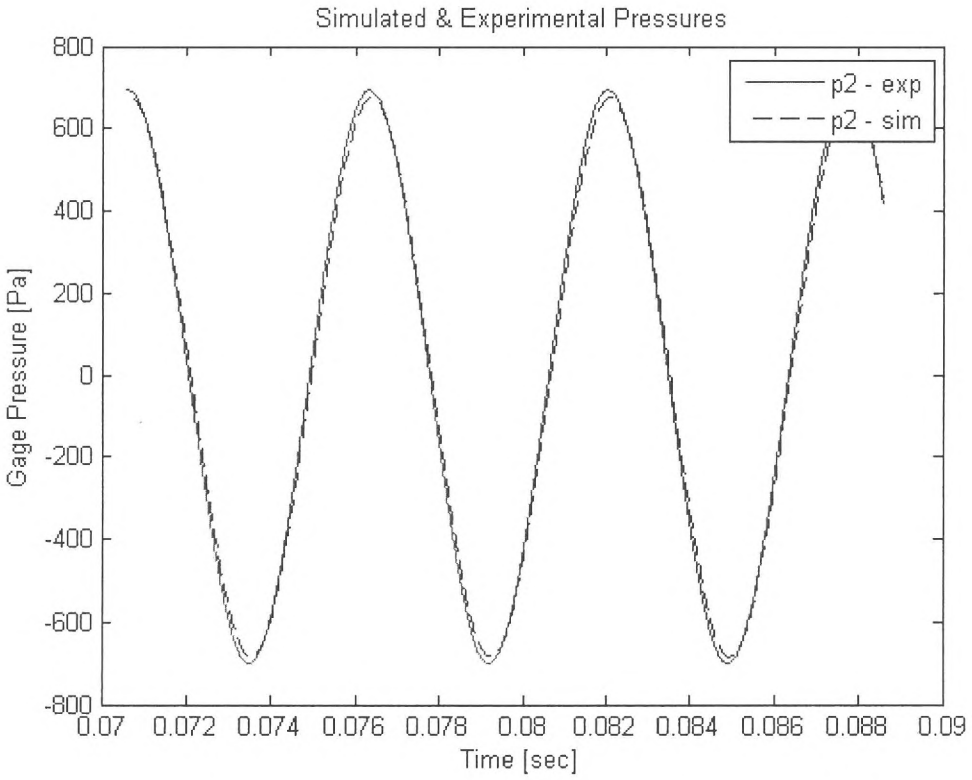

Figure 3.2.5: 635 stainless steel experimental and simulated periodic radial flow pressure plots for at 175 Hz (400 psig)

The iterative solution method produced a single set of radial flow parameters for each test sample at each pressure that showed good agreement for all the discrete frequencies. Results for the oscillatory flow radial hydrodynamic resistances, Darcy permeability, and Forchheimer's coefficients are summarized in Table 3.2.4.

Porous Media	Charge Pressure psig	Viscous Resistance 1/m^2	Inertial Resistance 1/m	Darcy Permeability m^2	Forchheimer's Coefficient ---
325 Phosphor Bronze	400	2.90E+10	50000	1.549E-11	0.327
325 Phosphor Bronze	490	2.90E+10	50000	1.549E-11	0.327
635 Stainless Steel	400	1.05E+11	120000	3.785E-12	0.466
635 Stainless Steel	490	1.11E+11	120000	3.596E-12	0.454
400 Stainless Steel (Sintered)*	400	1.50E+11	200000	2.563E-12	0.672

Table 3.2.4: Periodic Radial Flow Sample Hydrodynamic Parameters
*400 Stainless Steel Sintered Parameters [Cha 2007]

3.3 CFD Simulations

3.3.1 Simulations at Meso-Scale

Fluent models have been constructed of meso-scale inertance tube and reservoir-less inertance tube PTRs having the dimensions listed in Table 3.1.1, and have been tested. These models used a time steps of 20 μs, which for an operating frequency of 200 Hz worked out to 250 time steps per period of pressure oscillations. An operating pressure of 3.55 MPa was prescribed and an oscillating pressure with an amplitude of 0.25 MPa was applied by a user defined function at the inlet, resulting in a pressure ratio of 1.15, consistent with the Sage models.

Solid conduction in the regenerator and pulse tube shells was modeled by including these regions, as well as the warm and cold heat exchangers, in the CFD models. They were meshed and specified as solids with appropriate material properties. Wall thicknesses of the transfer lines, inertance tube, and reservoir volume were neglected, however, because their contribution to adverse heat conduction is small in comparison with regenerator and heat exchanger walls. Since hydrodynamic closure parameters for the regenerator fillers that have been chosen for the prototype meso – scale PTR were not available yet, the preliminary calculations were performed using stainless steel 400 mesh parameters. More reliable simulations based on the filler characterization test results are underway at this time

The CFD models were able to incorporate 2D effects that can not be modeled in Sage, such as tapering done to the inner and outer walls of the pulse tube. The inner diameter of the pulse tube was expanded from 2.5 mm in the center to 4 mm at either end, over a distance of 3 mm, in order to avoid the flow disruption caused by a step change in diameter. These dimensions, it should be emphasized, are the same as the dimensions of the prototype meso – scale PTR that is under construction at this time (See Section 3.4).

For the initial geometry, transferred straight from Sage without Fluent optimization or inertance length correction for proper phase shift, Fluent predicts ultimate no-load temperatures below 140 K for the standard inertance tube PTR and below 166 K for the

reservoir-less design. Figure 3.3.1 shows cycle-averaged temperature histories for the cold heat exchangers for the standard inertance tube PTR model started at 140 K and the reservoirless ITPTR model started at 170 K. Depicted in Figure 3.3.2 are enthalpy flow rate histories at the inlet and at each heat exchanger, as well as an overall enthalpy balance for the entire system. From these enthalpy balances it is evident that the models are converging towards periodic steady state as both of their balances are asymptotically approaching zero. While the models approach their periodic steady state solutions their cold heat exchanger temperatures continue to decrease.

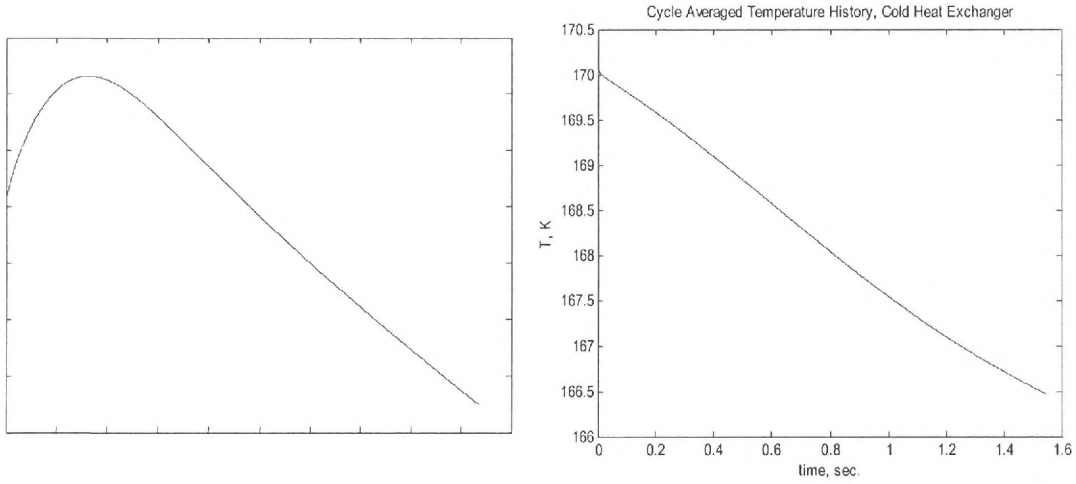

A) B)

Figure 3.3.1: cycle-averaged cold heat exchanger temperatures, meso-scale models A) ITPTR and B) Reservoir-less ITPTR

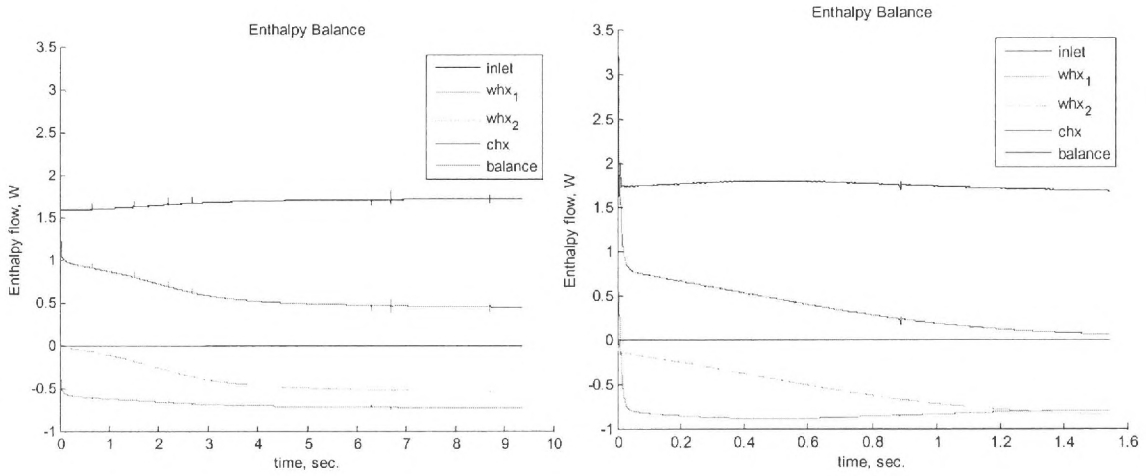

Figure 3.3.2: Enthalpy flow rates and overall enthalpy balances, meso-scale models. A) ITPTR and B) Reservoir-less ITPTR

Once the initial set of CFD models have reached periodic steady state, their inertance lengths will be optimized using Fluent to provide optimal phase shift, in order to further improve their performance. With both models operating optimally, subject to their initial geometry and the initial design constraints placed on them, it will then be possible to isolate the effects of changes to component dimensions and PTR operating conditions and perform more parametric optimization of them.

3.3.2 Simulations at Micro-Scale

As was done for the meso-scale PTRs, CFD models of micro-scale inertance tube and reservoir-less inertance tube PTRs have been constructed, and preliminary simulation tests have been performed. The dimensions of these models are also listed in Table 1. The total volume of the micro – scale PTR, as mentioned earlier, will be about 1 cubic centimeter. These models use a time steps of 10 μs, which for an operating frequency of 400 Hz works out to 250 time steps per period of pressure oscillations. For the initial, Sage derived geometry and operating conditions Fluent predicted ultimate no-load temperatures below 180 K and 200K for both standard and reservoir-less inertance tube PTR models, respectively. Cycle-averaged cold heat exchanger temperature histories for these micro-scale models are shown in Figure 3.3.3. Once converged to their periodic steady state solutions, the micro-scale models will be optimized in the exact same manner as their meso-scale counterparts.

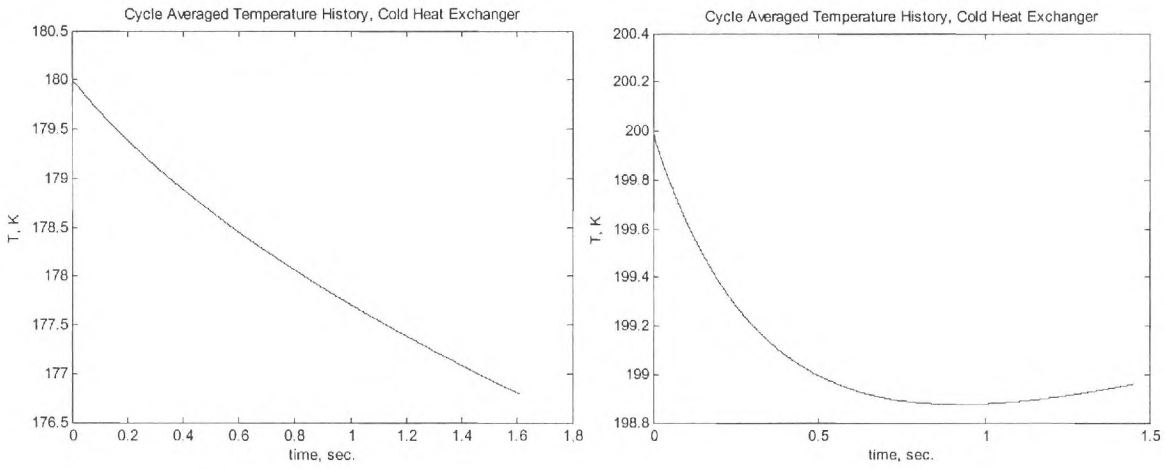

A) B)

Figure 3.3.3: Cycle-averaged cold heat exchanger temperature histories, micro-scale models. A) ITPTR and B) Reservoirless ITPTR

3.4 Prototype Manufacturing and Testing

A key element of the program is developing the appropriate mechanisms for fabricating small-scale pulse tube refrigerators in an effective manner for both performance and cost. Challenges in this regard include the fabrication of the mesh filler materials for both the regenerator and the heat exchangers and aftercooler and the integration and assembly of the mm scale diameter components in ways that are not detrimental to their functionality. The prototype miniature PTR described in this section is a meso-scale cryocooler that has a total volume of about 4 cubic centimeters, excluding the compressor. The design, construction and testing of a meso scale PTR will serve three important purposes. First, meso-scale PTRs are of interest in their own right, and are likely to have important applications. Second, this process will allow us to validate and verify our analytical tools and techniques. Third, fabrication, testing, and demonstration of a meso-scale PTR will provide us with valuable experience that we will be able to use in the design and construction of a mocro-scale PTR. (We define a micro-scale PTR as one that has a total volume of about 1 cubic centimeter or smaller, excluding the compressor.)

3.4.1 Mesh Filler Fabrication

As described previously in section 3.2, mesh filler layers are used in both the heat exchanger elements of the PTR and in the regenerator itself. For the miniaturized prototype, it was deemed likely that 325 mesh phosphor bronze would be suitable for the heat exchangers and 635 mesh stainless steel would be suitable for the regenerator with the cutouts used in the mesh characterization shown in Figure 3.4.1. These materials are denser meshes than typically used for full-scale PTRs but are expected to be necessary to achieve the needed heat transfer characteristics over the small dimensions available for the device. Although possible MEMS fabricated regenerator elements have been given consideration during the program and have been previously demonstrated in the literature using patterning of nickel and photoresist layers (Moran, Stelter, and Stelter, 2004), it was deemed more critical to focus on conventionally available components which could be readily characterized and have proven utility in cryocooling devices.

While the mesh material selection was set, the fabrication approach still had to be determined. The denser weave meshes inherently have lower thicknesses thus requiring a large number of individual cut-outs to be made in order to pack the desired overall length. Two possibilities were considered for potential batch fabrication of mesh cuts to minimize the investment in labor or machinery involved in the conventional die cutting approach. The first was wire electrical discharge machining (EDM) of the appropriate shapes. The key advantage of wire EDM was the possibility of fabricating very large stacks of mesh layers with a single cutting pass thus massively reducing machining time and potentially allowing a pre-stacked set of mesh layers to be created instantly. A second possibility was

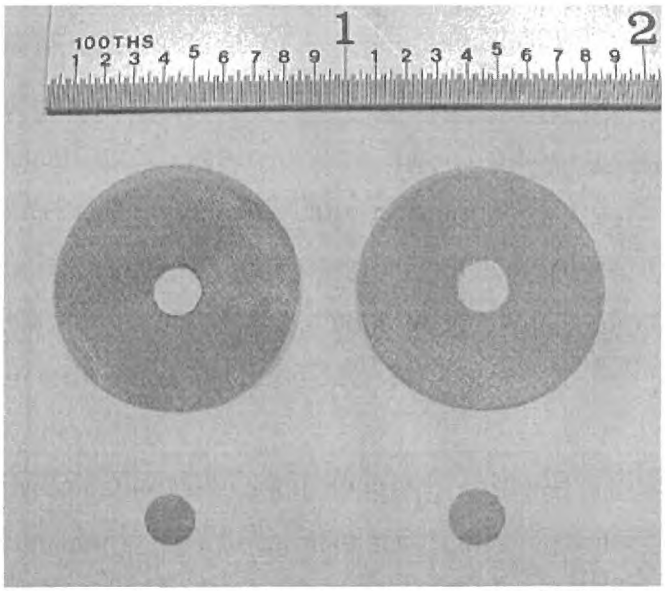

Figure 3.4.1: Mesh filler material test pieces fabricated through die punching for 635 stainless steel (left) and 325 phosphor bronze (right) with 4 mm o.d. axial flow cut-outs (below) and 20 mm o.d. by 4 mm i.d. radial flow cut-outs (above).

the use of laser cutting. In this approach, a Q-switched YLF laser would be used to cut through the thin mesh and repeat the cutout pattern over a large swatch of mesh material. While requiring significantly more time than wire EDM, laser cutting would still provide high tolerances on the cut sizing and minimize labor.

Sample cuts using all three fabrication approaches were performed in 325 stainless steel mesh with simple 0.25" diameter round cuts. (This material was readily available and significantly less expensive than the actual test materials.) Three microscope images at varying levels of magnification are shown in Figure 3.4.2 for wire EDM fabrication of a 30 layer stack of the mesh material. The individual mesh cut-outs released successfully from one another following the single cutting pass eliminating concerns that the individual layers would be effectively welded together due to the local heating at the arc discharge. However, the material did show a noteworthy effect from the heating with significant melting at the periphery of the cut yielding some distortion in the shape and some filling of the otherwise open spaces in the mesh with melted material. This result presents two problems as the disturbance to the regular mesh structure is likely to change the flow and heat transfer characteristics around the edge of the mesh and may also create loose pieces which might dislodge and create disruptions elsewhere in the filler. While the melting impact was confined to a very small area near the cut, this effect would

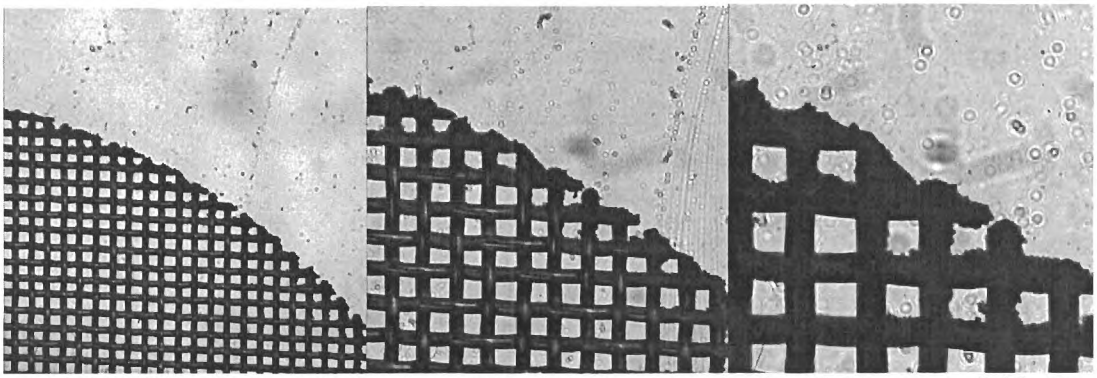

Figure 3.4.2: 325 stainless steel mesh cutouts fabricated through wire EDM process (30 layers stacked) shown at three different magnification levels.

become disproportionately larger for the small diameter (4 mm or less) cuts required for the meso- and micro-scale PTRs. A similar but slightly more pronounced melting effect was observed for the laser cut test pieces due again to local heating at the cutting location. By contrast, the die cut pieces (shown again for 3 levels of microscope magnification in Figure 3.4.3) showed no comparable distortion at the periphery of the cut except for a slight bevel at the exact cutting location. For this reason, it was deemed

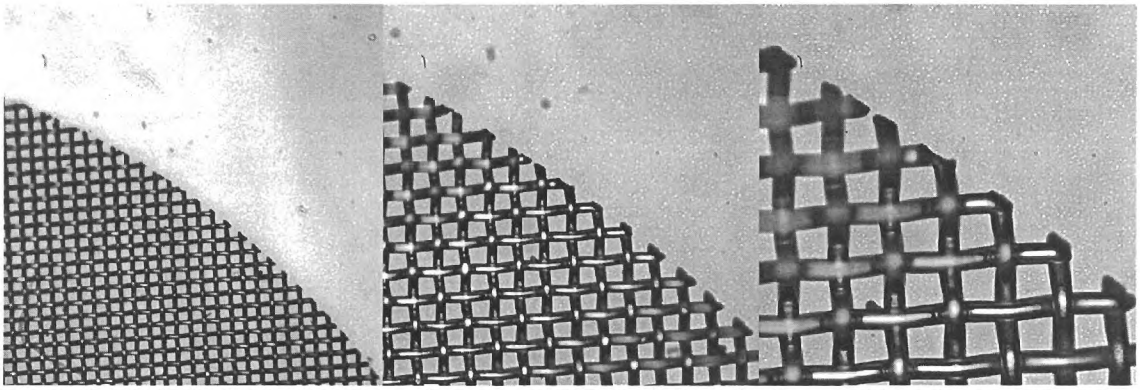

Figure 3.4.3: 325 stainless steel mesh cutouts fabricated through die punching shown at three different magnification levels.

preferable to use die cutting at least for the present experiments and the mesh fillers for the program were all die cut by hand. Should mass fabrication become desirable, a suitable feeding and hydraulic or pneumatic punching system could be devised to minimize manual labor.

3.4.2 Experimental Miniature PTR Prototype Fabrication

For the purposes of creating an experimental miniature (meso-scale) prototype in Phase I, dimensions for the PTR components were chosen early in the program based upon scoping design calculations using the SAGE program and the availability of off the shelf components at the correct sizing. An internal diameter of 4 mm was selected for all mesh-filled components (regenerator and heat exchangers) so that the cut-outs created for

the axial mesh filler characterization could be reused directly in the prototype testing. This 4 mm dimension typically guided the other dimensions as they scaled accordingly. An assembly layout of the initial prototype is shown in Figure 3.4.4. The total volume of the depicted PTR system, as mentioned earlier, is about 4 cubic centimeter. The material selection for the components was based in part on literature regarding previous small-scale PTRs and on component availability. For the pulse tube and regenerator, polyetheretherketone (PEEK) material was chosen for its good thermal insulation and machinability. Both components were fabricated from 0.25" rod stock of PEEK, with the regenerator section bored out to a 4 mm inner diameter and the 0.25" (6.35 mm) outer diameter maintained. The regenerator section length is 21 mm and each end includes a counterbored step 1.2 mm deep for mating with the adjacent aftercooler and cold heat exchanger. The pulse tube itself has 4 mm inner diameter at both ends but tapers down to a 2.5 mm diameter over the majority of its length. Likewise, the pulse tube outer diameter tapers down from a 6.35 mm o.d. to a 3.9 mm o.d. in the central section. The active length of the device is 39 mm with similar counterbored steps at the ends allowing mating to the cold and war heat exchangers.

The aftercooler and heat exchangers for the system were fabricated from sterling silver tubing with an inner diameter of 4.0 mm and an outer diameter of 4.8 mm. This is a novel approach as copper heat exchanger walls are typically used. The thermal conductivity of silver is in fact 7% higher than that of copper (429 vs. 401 W/m·K), but silver is rarely used in large scale heat exchanger systems due to the significantly higher

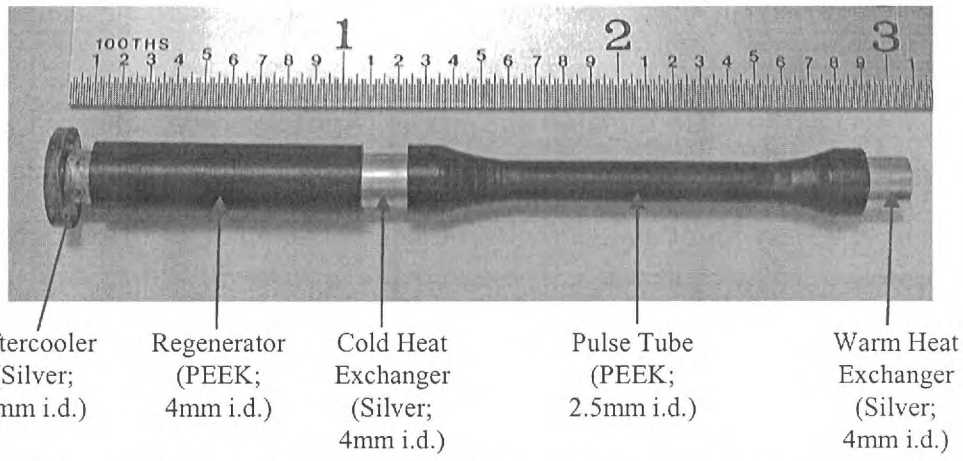

Figure 3.4.4: Prototype miniature PTR components in initial assembly layout.

material cost. At the scale of the present device, however, the cost penalty is minimal (although this might require further consideration should successfully demonstrated miniature PTRs be placed into mass production). An additional factor in the choice of silver was the possibility of finely controlled silver soldering techniques to be used to bond the mesh filler materials to the heat exchanger walls. (Initial attempts at this have proved problematic as any excess amount of solder on the walls can easily flow into the mesh material and fill the open spaces changing the flow characteristics. This approach may be given future consideration when more controlled means of creating a very thin solder layer on the walls – perhaps through sputtering or other microfabrication approaches – can be investigated more fully.) For the warm and cold heat exchangers, the total length is held to 5 mm, and for the aftercooler, the length is 6 mm (although shown in Figure 3.4.4 with a copper flange attached, the actual final aftercooler will be attached to a larger copper heat exchanger plate as part of the vacuum dewar system to be described below).

Full assembly of the device has not yet taken place at the time of this draft report, and will be accomplished pending the acquisition of the mesh screens for loading into the components. The mesh screens will be thoroughly cleaned prior to assembly to eliminate any contaminants and the assembly will take place in a clean room environment with mesh inserted into the aftercooler, followed by the epoxy attachment of the regenerator, loading of the regenerator mesh, epoxy attachment of the cold heat exchanger, loading of the cold heat exchanger mesh, epoxy attachment of the pulse tube, epoxy attachment of the warm heat exchanger and the loading of its screens, and finally epoxy attachment of an end cap. Around each set of mesh screens will be a single coarser mesh cutout designed to contain the screens and eliminate the possibility of any movement or loosening of the screens in response to the pressure waves within the system.

The use of epoxy to attach the components will be another novel element of this prototype as conventional PTRs use flanges and o-rings/gaskets for sealing and mechanical attachment. However, at the scales of the present device, any mechanically

useful flange design becomes so relatively large as to significantly alter the thermal inertia of the component it is attached to (see the test flange on the aftercooler in Figure 3.6.4). Also, mechanical attachment is more critical for larger devices due to the high pressure forces pushing the elements apart. For this device, even at 400 psi filling pressure, only a 6 lb force must be resisted to maintain attachment, placing it well within the range of adhesives and epoxies. The final choice of the attachment epoxy is still under investigation in order to insure that no significant outgassing is possible through the junctions. Many adhesives and epoxies are previously demonstrated resistant outgassing (cataloged, for example, in the NASA outgassing database - http://outgassing.nasa.gov/) although confirmation is being sought that these results extend to helium processes. An additional initial concern regarding the use of epoxies was the possibility of thermal expansion/contraction weakening the epoxy junctions between the components. A finite element analysis of the thermal properties of the entire device is underway in the COSMOS FEA package using estimated temperatures throughout the device. However, initial calculations of the displacement in the axial direction suggest that the thermal expansion should be well within the tolerance of the epoxy. For example, setting the cold heat exchanger to 50 K from an initial room temperature state yields a thermal contraction of only 23.3 μm. Even smaller changes are expected to occur in other components as only small temperature changes are expected for each.

Beyond the prototype itself, fabrication is currently on-going for a vacuum dewar system that will form the outer housing of the device and allow for isolated measurements from the external device. A schematic of the assembled prototype and dewar is shown in Figure 3.4.5. The entire test facility is only 2.5" in diameter by approximately 6" long. The bottom plate is a copper heat exchanger surface into which the aftercooler is mounted and will likely be held with thermally conductive silver epoxy. Through the copper plate runs a single loop of copper tubing for running water through the system to carry away heat from both the aftercooler and warm heat exchanger. At the ends of the cylinder at pass through for the small 1/16" line connections of the compressor and inertance line. The inertance line connection (top of Figure 3.4.5) is through a vacuum fitting which will allow some variation in the total length of the PTR components for future use with other designs. The two fittings on the side wall are for the vacuum line connection and hermetic insertion of thermocouples and other sensors into the dewar.

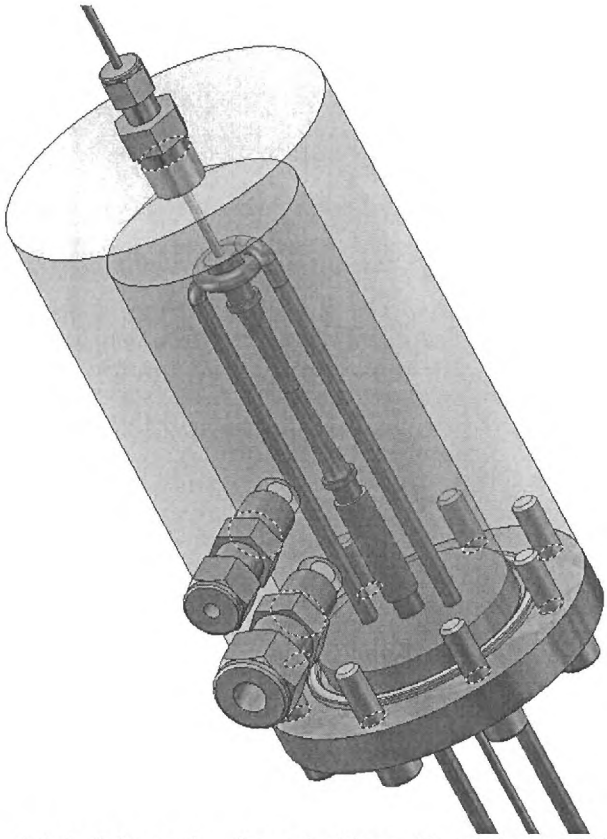

Figure 3.4.5: Schematic of test facility with miniature PTR, copper base plate and heat exchanger loop, and outer vacuum dewar.

3.4.3 Initial Prototype Test Results

Although it is desired to be able to make preliminary tests with the prototype before the final close of this Phase 1 program, reliable and verified prototype test results may not be realistically anticipated until the final close of the program. In addition, the

operating parameters of the currently available compressor system (regarding either the frequency or achievable pressure ratio) may ultimately prove unsuitable for operation at the prototype scale. Simple tests of the prototype will be performed in the fabricated vacuum dewar, however, to investigate several key questions. Of primary interest will be confirming the suitability of the fabrication approach for the device, including demonstrating successful assembly and insuring that no leakage is observed from any of the system elements at operating pressures and temperatures.

Although this miniature PTR design was created from limited data and partially in response to constraints regarding the mesh filler sizes for the characterization set-up, our most conservative simulations indicate that it must be able to reach low-end temperatures of around 140 – 160 K, when the warm end is at room temperature. (Sage simulations actually suggest cold minimum end temperatures as low as about 100 K.) Careful simulations also indicate that the system performance is sensitive to some design details, most importantly the phase shift arrangement. Thus, although this level of cooling will make the design suitable for staged cryocooling applications, we expect the performance of an optimized meso – scale PTR to be significantly better. These simulation results of course need experimental verification. However, any observed results should provide useful feedback for future simulations and provide an experimental baseline from which to refine the design in future work.

4. CONCLUSIONS

Concluding Remarks

This Phase I investigation was aimed at the design and proof-of-concept demonstration of meso and micro scale PTR systems. As part of the investigation, the following objectives were successfully achieved.

1. Extensive parametric and optimization simulations were performed using SAGE. The tentative outcomes of these analyses and optimizations for meso and micro – scale PTRs were then verified by detailed CFD simulations.
2. Based on the above simulations, inetance-tube based and reservoirless meso and micro – scale PTRs systems (excluding the compressor) were designed, with total volumes (excluding the compressor) of approximately $4\,cm^3$ and $1\,cm^3$, respectively. The system design process included the selection of appropriate fabrication materials. For the meso – scale PTRs operating at 200 Hz with their warm heat exchangers in room temperature, no – load temperatures below 140 K for the standard inertance tube PTR and below 166 K for the reservoir-less design were conservatively predicted. For the micro – scale PTRs operating at 400 Hz, the corresponding conservatively – predicted no – load temperatures were 180 K and 200K, respectively. It was thus concluded that meso and micro scale PTRs are feasible at least for staging applications.
3. A review of commercially available filler materials for regenerators and heat exchangers was carried out. It was determined that 635 wire mesh stainless steel screens are suitable for miniature regenerators, while 325 phosphor bronze wire mesh screens can be used for miniature heat exchangers. Since the hydrodynamic parameters associated with the flow of helium in these fillers are currently unknown, experiments were performed in which the anisotropic (axial and radial – directions) hydrodynamic closure parameters for these two filler materials were measured. These parameters can be used in the future for the final CFD design and optimization simulations of meso and micro scale PTRs.
4. Based on the above meso – scale simulations, a prototype PTR system (excluding the compressor was thoroughly designed and fabricated. The prototype PTR has a total volume (excluding the compressor) of slightly less than $4\,cm^3$. The regenerator and pulse tube are made from PEEK, and the heat exchanges and the aftercoler are made of silver. The prototype has been tested for …..

Accordingly, we conclude that meso and micro scale PTRs are feasible at least for staging applications, where small thermal loads can be disposed of and local temperature reductions of up to about 150 K can be implemented with a meso – scale PTR. With a micro – scale PTR, furthermore, staging applications with temperature reductions of up to about 80 K appear to be feasible.

5. RECOMMENDATIONS

While full recommendations can only be made following the completion of the CFD simulations and initial prototype testing, it is reasonable to state with confidence that mini and micro scale PTRs are feasible, at least for staged applications. It is also reasonable to assume that the FLUENT based modeling will more accurately capture the small-scale characteristics than the SAGE modeling and prove to be a critical tool for further design and optimization of PTRs in the meso- and micro-scale ranges. Further refinement will be necessary to provide the most accurate simulations possible and should involve an iterative process of optimization whereby the CFD models provide a recommended design, this design is experimentally fabricated and tested, and the experimental results used to update the model accordingly and again update preferred experimental design parameters. This interactive numerical/experimental process is feasible now that basic modeling of the system has been achieved and scale – appropriate experimental prototyping procedures have been demonstrated and should form the core of a follow-on Phase II program to fully apply these results.

During this program, other key design parameters could be considered, including various alternative overall PTR system designs (e.g., coaxial), and specific loading and inlet conditions that accurately represent initial technology transition applications for miniature PTRs. An example of this would be a multi-staged cryogenic system where one or more large-scale cryocoolers carry the bulk cooling load at a given temperature and miniature PTRs are used to stage the system to even lower reservoir temperatures to meet specific smaller thermal requirements for infrared sensors, etc. This concept is more efficient than the current approach (carrying the full thermal load at below the operationally required temperature) but will require updates to the modeling to reflect changes to the rejection temperature and other parameters. Further consideration could also be given to redesign and optimization of various subsystems in the PTR including enhanced regenerator matrices (possibly including MEMS fabricated elements), optimized phase shift mechanisms for the miniature devices, and innovative concepts for reducing both thermal and frictional losses. Finally, the modeling and experimentation

could provide confirmed results regarding the minimum scales at which a micro-PTR cryocooler is feasible. All of the above elements would be of significant technical and scientific value and would each be considered under a Phase II program.

REFERENCES

Cha, J. S., 2007. "Hydrodynamic Parameters of Micro Porous Media for Steady and Oscillatory Flow: Application to Cryocooler Regenerators" Ph.D. Thesis, Georgia Institute of Technology, Atlanta, GA.

Cha, J.S., Ghiaasiaan, S.M., and Kirkconnel, C.S., 2008. "Oscillatory Flow Anisotropic Hydrodynamic Parameters of Microporous Media Applied in Pulse Tube and Stirling Cryocooler Regenerators," Exp. Thermal Fluid Science (in press).

FLUENT 6 Users Manual, Fluent Inc., 2003.

Garaway, I and Grossman, G, 2007 "A Study of High Frequency Miniature Reservoir-less Pulse Tube" CEC/ICMC 2007, Chattanooga, TN.

Gideon, D., 1999. *SAGE: Pulse Tube Model Class Reference Guide,* Gideon Associates.

Herwig, H., and Hausner, O. , 2003, Critical View on "New Results in Micro-fluid Mechanics": an Example. Int. J. Heat Mass Transfer, 46, 935-937.

Liang, J., Zhou, Y., Zhu, W., Sun, W., and Li, Y.S., 2000, "Study on Miniature Pulse Tube Cryocooler for Space Application," Cryogenics, 40, 229-233.

Moran, M., Stelter, M., and Stelter, S., 2004, "Micro-scale Regenerative Heat Exchanger," AIAA Paper 2004-6730.

Nika, P., Bailly, Y., de Labacherie, M., Jeannot, J.C., and de Lallee, J., 2004, "Miniature Pulse Tube for the Cooling of Electronic Devices: Functioning Principles and Practical Modeling," Microscale Thermophysical Engineering, 8, 301-325.

Tiselj, I., Hetsroni, G., Mavko, B., Mosyak, A., Pogrebnyak, E., and Zegal, Z., 2004, Effect of Axial Conduction on the Heat Transfer in Micro-channels. Int. J. Multiphase Flow, 47, 2551-2565.

Tward, E., Chan, C.K., Jaco, C. , Goddard, J., Chapsky J., and Clancy, P., 1999, "Miniature Space Pulse Tube Cryocoolers," Cryogenics, 39, 717-720.

Waldauf, A., Thurke, M., and Seidel, P., 2004, "Observation and Control of Temperature Instabilities in a Four-Valve Pulse Tube Refrigerator," Cryogenics, 44, 75-79.

Xu, M., He, Y., Wu, P., and Chen, Z., 1996, "Experimental Research of a Miniature Coaxial Pulse Tube Refrigerator Using Nylon Tube," Cryogenics, 36, 131-133.

Yu, Y.L., Wang, C., and Zhou, Y., 1998. "Numerical Simulation and Experimental Verification of the Oscillating Flow in Pulse Tube Refrigerator," Cryogenics, 28, 169-176.